YhcB coordinates peptidoglycan and LPS biogenesis with phospholipid synthesis during *Escherichia coli* cell growth.

Emily C. A. Goodall[a], Georgia L. Isom[b], Jessica L. Rooke[a], Christopher Icke[a], Karthik Pullela[a], Bing Zhang[a], James Rae[a], Wee Boon Tan[c], Matthias Winkle[d], Antoine Delhaye[e], Eva Heinz[f], Jean-Francois Collet[e], Adam F. Cunningham[b], Mark A. Blaskovich[a], Robert G. Parton[a g], Jeff A. Cole[b], Shu-Sin Chng[c], Waldemar Vollmer[d], Jack A. Bryant[b], Ian R. Henderson*[a]

[a] Institute for Molecular Biosciences, The University of Queensland, St. Lucia, Australia

[b] Institute of Microbiology and Infection, University of Birmingham, UK

[c] Department of Chemistry, National University of Singapore, Singapore

[d] Centre for Bacterial Cell Biology, Biosciences Institute, Newcastle University, Newcastle upon Tyne, UK

[e] de Duve Institute, UCLouvain, Brussels, Belgium

[f] Departments of Vector Biology and Clinical Sciences, Liverpool School of Tropical Medicine, Liverpool, UK

[g] Centre for Microscopy and Microanalysis, The University of Queensland, St. Lucia, Australia

*Corresponding author: i.henderson@imb.uq.edu.au

Running title: YhcB coordinates peptidoglycan and LPS export with phospholipid synthesis

Keywords: YhcB, cell envelope, polymyxin B, *Escherichia coli*, LPS, peptidoglycan, phospholipid membrane, TraDIS, TIS, transposon mutagenesis

Abstract

The cell envelope is essential for viability in all kingdoms of life. It retains enzymes and substrates within a confined space while providing a protective barrier to the external environment. Destabilising the envelope of bacterial pathogens is a common strategy employed by antimicrobial treatment. However, even in one of the most well studied organisms, *Escherichia coli*, there remain gaps in our understanding of how the synthesis of the successive layers of the cell envelope are coordinated during growth and cell division. Here, we used a whole genome phenotypic screen to identify mutants with a defective cell envelope. We report that loss of *yhcB*, a conserved gene of unknown function, results in loss of envelope stability, increased cell permeability and dysregulated control of cell size. Using whole genome transposon mutagenesis strategies we report the complete genetic interaction network of *yhcB,* revealing all genes with a synthetic negative and a synthetic positive relationship. These genes include those previously reported to have a role in cell envelope biogenesis. Surprisingly, we identified genes previously annotated as essential that became non-essential in a Δ*yhcB* background. Subsequent analyses suggest that YhcB sits at the junction of several envelope biosynthetic pathways coordinating the spatiotemporal growth of the cell, highlighting YhcB as an as yet unexplored antimicrobial target.

Introduction

The bacterial cell envelope plays a fundamental role in protection, host interaction, energy generation, expulsion of toxic substances and coordination of growth and cell division. As a physical barrier, it has a central role in acquired and intrinsic antimicrobial resistance. The cell envelope biogenesis systems are therefore important drug targets. In Gram-negative bacteria, the tripartite cell envelope is composed of the cytoplasmic membrane (CM), peptidoglycan (PG) layer and an outer membrane (OM) (Silhavy et al.

2010). The OM is an asymmetrical bilayer of phospholipids and lipopolysaccharide (LPS), which forms a strong permeability barrier conferring resistance to many toxic antimicrobials. Both membranes are studded with integral membrane proteins and peripheral lipoproteins that facilitate cellular functions (Lugtenberg 1981; Molloy et al. 2000; Luirink et al. 2012). Each component of the cell envelope must be synthesised and assembled in a coordinated fashion to maintain cell envelope homeostasis and viability. Thus, understanding how this complex envelope is synthesised and maintained is instrumental to understanding how to disrupt its function, to kill the bacterium, or render the organism susceptible to otherwise ineffective treatments.

Over the last 50 years a variety of sophisticated and complex multiprotein machineries have been discovered that are required for the synthesis of the Gram-negative cell envelope. The Lpt machinery facilitates insertion of LPS into the OM (Sperandeo et al. 2008; Polissi and Sperandeo 2014; May et al. 2015; Simpson et al. 2015; Okuda et al. 2016; Sherman et al. 2018), the BAM complex coordinates OM protein assembly and insertion (Ruiz et al. 2005; Wu et al. 2005; Knowles et al. 2009), the Lol system traffics lipoproteins across the periplasm for incorporation into the OM (Matsuyama et al. 1995; Matsuyama et al. 1997; Yakushi et al. 2000; Okuda and Tokuda 2011), the Mla complex enables phospholipids transport between the two membranes (Malinverni and Silhavy 2009; Thong et al. 2016; Abellón-Ruiz et al. 2017; Powers and Trent 2018; Ercan et al. 2019; Hughes et al. 2019; Shrivastava and Chng 2019; Chi et al. 2020), and the elongasome and divisome are the architects of peptidoglycan assembly during cell elongation and division (Goehring and Beckwith 2005; Den Blaauwen et al. 2008). Each pathway in isolation is broadly understood. However, the precise molecular events that govern the crosstalk between the different biosynthetic pathways, both spatially and temporally during growth and cell division, remain to be elucidated.

78 Genetic screens to identify synthetically lethal interactions and suppressor
79 mutations have played a significant role in identifying the interconnected pathways of
80 envelope biosynthesis (Ogura et al. 1999; Klein et al. 2014). Transposon insertion
81 sequencing (TIS) is one approach that enables the study of genetic interactions on a
82 whole genome scale (DeJesus *et al*. 2017). Here we used a chemical genomics approach
83 to identify genes required for cell envelope homeostasis in *Escherichia coli,* coupling
84 TraDIS, a TIS method (Langridge et al. 2009; Cain et al. 2020), with the membrane
85 targeting antibiotic polymyxin B. We demonstrate that a poorly characterised protein,
86 YhcB, is crucial for tolerance to polymyxin B and for maintenance of cell envelope
87 homeostasis in *E. coli*. Previous studies revealed that YhcB is a CM protein widely
88 conserved in Gammaproteobacteria that physically interacts with the elongasome, the
89 machine that coordinates peptidoglycan synthesis along the cylindrical part of the cell,
90 and with LapA, a protein involved in regulating LPS biosynthesis (Mogi et al. 2006; Den
91 Blaauwen et al. 2008; Maddalo et al. 2011; Li et al. 2012; Klein et al. 2014; Mahalakshmi
92 et al. 2014; Fivenson and Bernhardt 2020). We demonstrate that loss of YhcB results in
93 dysregulation of cell length and width. We created a high-density transposon mutant
94 library in an *E. coli* Δ*yhcB* strain to gain a whole genome view of genetic interactions with
95 *yhcB*. Subsequent screening of this library against chemical stresses revealed all genes
96 that suppress the envelope defects associated with the loss of *yhcB.* These data suggest
97 that YhcB is stationed at the interface between PG and LPS synthesis, and phospholipid
98 membrane biogenesis, and has a role in coordinating the spatial and temporal assembly
99 of the cell envelope.
100
101 **Results**
102 ***Identification of envelope barrier-defective mutants***

103 Previously, we described a high-density transposon-mutant library of *E. coli* K-12
104 (Goodall et al. 2018). To identify genes required for cell envelope biogenesis we applied
105 a chemical genomics approach exposing our library to sub-inhibitory concentrations of
106 the membrane-acting antibiotic polymyxin B (Fig. S1A). Polymyxins bind the lipid A
107 moiety of LPS, displacing divalent cations, disrupting the integrity of LPS-crosslinks, and
108 resulting in an increase in membrane permeability (Newton 1953; Dixon and Chopra
109 1986; Trimble et al. 2016; Li and Velkov 2019). We posited that if the transposon disrupts
110 a gene required for the maintenance of cell envelope integrity, the resulting mutant will
111 become more susceptible to polymyxin B, and the gene would be identified through our
112 TIS screen as these mutants will be outcompeted during growth; identifiable as a
113 depletion in transposon-insertions. We grew the transposon library in LB broth with or
114 without 0.2 µg/ml polymyxin B, in duplicate, and harvested cells after ~5 generations of
115 growth (Fig. 1A). The sequencing yielded a total of >4.2 M reads, estimated to sample
116 >99% of the possible unique insertion sites (Fig. S1B). We used the BioTraDIS pipeline
117 for data processing and analysis (Barquist et al. 2016), and mapped the processed reads
118 to the *E. coli* BW25113 reference genome obtained from NCBI (accession CP009273.1).
119 The insertion index scores (IISs; the number of insertions per gene, normalised for gene
120 length) between replicates were highly comparable (Fig. S1C). We identified 54 genes
121 required for growth in sub-inhibitory concentrations of polymyxin B (Fig. 1B; Table S1).
122 Comparison of the relative abundance of COG (Cluster of Orthologous Groups)
123 categories of these 54 genes showed a marked increase in genes involved in cell
124 wall/membrane/envelope biogenesis (COG category 'M'), supporting the validity of the
125 TIS screen (Fig. S1D). Many of these genes (e.g. *bamB*, *degP*, *galE*, *surA*, and
126 *waaBCFGJPR*) have been identified in a similar TIS screen using *Klebsiella pneumoniae*
127 or have previously been reported as mutants sensitive to polymyxin (Yethon et al. 2000;
128 Jana et al. 2017). The COG analysis identified only three genes (*ydbH*, *yqjA* and *yhcB*)

129 of unknown function (category 'S' in Fig. S1D) that were important for survival when
130 exposed to sub-inhibitory concentrations of polymyxin B (Fig. 1C and Fig. S1E). YdbH is
131 a putative autotransporter, while YqjA belongs to the DedA family of proteins that have
132 been suggested to be involved with membrane homeostasis (Keseler et al. 2017). Given
133 that *yhcB* is conserved in three out of the six ESKAPE pathogens, is required for tolerance
134 to polymyxin, an antibiotic of last resort, and is the target of a sRNA toxin that causes cell
135 death, we decided to investigate the role of YhcB further (Mogi et al. 2006; Choi et al.
136 2018).
137
138 ***Deletion of* yhcB *confirms an envelope defect***
139 To confirm the barrier defect of the *yhcB* mutant, we grew the parent strain, *E. coli*
140 BW25113, and an isogenic Δ*yhcB* mutant on LB agar plates supplemented with either
141 vancomycin, a high molecular weight antibiotic that is typically unable to cross the Gram-
142 negative OM, or plates supplemented with SDS and EDTA (Nikaido and Vaara 1985;
143 Nikaido 2005). The Δ*yhcB* mutant was more sensitive than the parent strain to both
144 conditions (Fig. 2A). Ectopic expression of YhcB under arabinose induction on a pBAD
145 plasmid was able to complement sensitivity defects, consistent with previous reports
146 (Sung et al. 2020). These data confirm that loss of *yhcB* results in a severe envelope
147 defect (Fig. S2A).
148
149 ***Effect of YhcB on cell size***
150 Despite normalising cultures by optical density, the number of viable colony
151 forming units (CFUs) of the Δ*yhcB* mutant were 10-fold fewer than the parent on the LB
152 control plate (Fig. 2A). Analysis of cellular morphology by DIC microscopy revealed that
153 the Δ*yhcB* mutant cells were significantly larger than the parent strain when grown in LB
154 (Fig. 2B). Expression of *yhcB* in the Δ*yhcB* mutant background substantially decreased

155 the cell dimensions relative to the Δ*yhcB*-pBAD empty vector strain but did not restore
156 cell size completely (Fig S2B). We also observed that the ectopic expression of *yhcB* in
157 the *E. coli* BW25113 parent strain resulted in longer cells than the control. Taken together,
158 these data suggest that the abundance of YhcB within the cell impacts cellular
159 dimensions, and that YhcB is important for maintaining cell size and shape.

160 Bacterial cell dimensions are influenced by a number of factors (reviewed by Cesar
161 and Huang 2017), but cell size is fundamentally determined by growth rate and nutrient
162 availability (Schaechter et al. 1958; Hill et al. 2013; Vadia and Levin 2015; Vadia et al.
163 2017). A shift from growth in nutrient-restricted to nutrient-rich medium results in an
164 increase in both cell length and cell width (Pierucci 1978). Therefore, we investigated the
165 effect of growth medium on the size of the Δ*yhcB* mutant. Overnight growth in M9 minimal
166 medium supplemented with glucose (M9-glucose) substantially decreased the cell size
167 of the Δ*yhcB* mutant compared to growth in LB, although a small subset of cells within
168 the population still exhibited a division defect and increased cell length (Fig. 2B-C).
169 Moreover, overnight growth in M9-glucose restored resistance to membrane-acting
170 compounds SDS and EDTA, but cells remained susceptible to vancomycin (Fig. 2A).
171 Changes in temperature alter growth rate but not size (Schaechter et al. 1958). To
172 understand whether the fitness advantage conferred by growth in M9-glucose was due
173 to a slower doubling time, or nutrient-dependent, we grew the Δ*yhcB* mutant in a range
174 of conditions. Overnight growth in M9-glucose and M9-glycerol at 37˚C, and LB at 16˚C,
175 restored resistance to both SDS and EDTA, but no growth condition conferred resistance
176 to vancomycin (Fig. S3). Altogether these results indicate that a slower growth rate
177 partially alleviates the defect caused by deletion of *yhcB* but does not restore the
178 envelope permeability barrier.

179 We hypothesised that there is an envelope synthesis defect in a Δ*yhcB* mutant that
180 becomes more severe over time during growth in LB. To investigate this, overnight

181 cultures (grown first in M9 medium) were sub-cultured in LB at a starting optical density
182 (OD) of 0.05. Bacteria were grown at 37˚C with aeration, and both the OD_{600} and the
183 corresponding number of CFUs were recorded hourly. The rate of increase in biomass of
184 the mutant, as assessed by optical density, was comparable to that of *E. coli* BW25113
185 (Fig. 3). In contrast, upon transition to stationary phase, the number of Δ*yhcB* CFUs
186 decreased 10-fold from ~3.5×10^8 to ~3.5×10^7. These data suggest that the fast-growing
187 mutant cells gradually expand in cell size, fail to divide, but lose viability when they enter
188 the stationary growth phase.
189
190 ***The domains of YhcB contribute to survival under different conditions***
191 To gain a better understanding of how YhcB functions, we scrutinised the primary
192 structure of the protein. A prediction of YhcB secondary structure of YhcB by PSIPRED
193 supports the model put forward by Mogi et al. (2006; Jones 1999; Buchan and Jones
194 2019). YhcB has a single transmembrane (TM) domain, with a cytoplasmic helical domain
195 and a disordered cytoplasmic C-terminal region (Fig. S4A); the topology of which has
196 been confirmed by GFP- and PhoA-fusion analysis (Maddalo et al. 2011). A
197 multisequence alignment of the amino acid sequence of YhcB from 150 different species
198 was generated using the online program ConSurf (Ashkenazy et al. 2016). This revealed
199 two highly conserved amino acid motifs within the disordered C-terminus: a 'NPF' motif
200 after the long cytoplasmic helical domain, followed by a non-conserved linker region, and
201 a highly conserved 'PRDY' motif at the extreme C-terminus (Fig S4B). A large number of
202 transposon insertions were identified within the 3′ end of *yhcB* in the initial polymyxin TIS
203 screen; the *yhcB* gene only met the stringency criteria for identification when 20% of the
204 3′ end of the coding sequence (CDS) was discarded. We mapped the coordinates of
205 these domains to the original TIS data and the data suggest that the 'PRDY' domain is
206 dispensable for survival in the presence of polymyxin B (Fig. 4A). To confirm the

207 functional importance of the 'PRDY' domain, which is highly conserved (Fig. S5), we
208 constructed complementation vectors encoding truncated variants of YhcB and repeated
209 our plate-based envelope screens (Fig. 4B). Consistent with results reported by Sung *et*
210 *al*. (2020), the ΔTM construct fully complemented both phenotypes. However, deletion of
211 the 'PRDY' domain rendered the mutant sensitive to vancomycin, but not SDS-EDTA
212 (Fig. 4C). These data suggest a dual function of the YhcB protein: the cytoplasmic helical
213 domain is needed to suppress sensitivity to SDS and EDTA, while the function of the
214 'PRDY' domain is needed for survival in the presence of vancomycin, but not polymyxin
215 B or SDS and EDTA.
216
217 ***Identification of genetic interactions with* yhcB**
218 To identify all genes with a synthetically lethal relationship with *yhcB*, a transposon
219 mutant library was constructed in a Δ*yhcB* background using a mini Tn*5* transposon
220 encoding a kanamycin resistance gene. A second library was constructed in the *E. coli*
221 BW25113 parent strain using the same transposon as a control. Approximately 800,000
222 transposon-mutants were collected and pooled for each library. Two technical replicates
223 of each library were sequenced (Fig. S6A; Table S2). There was a high correlation
224 coefficient between the gene insertion index scores of each replicate for both libraries (R^2
225 = 0.93 and R^2 = 0.96 for the WT and Δ*yhcB* library respectively). The insertion sites were
226 evenly distributed around the genome (Fig. 5A and Fig. S6B), and the respective insertion
227 density amounted to an average of one insertion every 6.28 bp in the WT library, and one
228 insertion every 6.99 bp in the Δ*yhcB* library. We quantified insertions per CDS to identify
229 genes that were sparsely disrupted by transposon insertion events i.e. essential genes in
230 each genetic background (Barquist et al. 2016). There was an overlap of 382 essential
231 genes between the two datasets and these were not considered further (Fig. 5B).

232 Previously, Li *et al.* (2012) reported that the deletion of both *rodZ* and *yhcB* in
233 combination is lethal, genetically linking the elongasome with the function of YhcB. Our
234 data confirmed a synthetic lethal interaction between *rodZ* and *yhcB*. However, we
235 observed that only the 5′ end of the *rodZ* gene, corresponding with the cytoplasmic helix-
236 turn-helix and transmembrane domains of the RodZ protein, is essential in a *yhcB*
237 background (Fig. 5C). These domains are required for maintaining cell shape (Shiomi et
238 al. 2008; Bendezú et al. 2009). This result supports the validity of our approach.
239 Surprisingly, our bimodal analysis of the data revealed 28 genes that were predicted to
240 be essential in a WT library but no longer essential when *yhcB* is deleted (Fig. 5B, Table
241 S3). This list includes *ftsH* (Fig. S6C), which encodes a metalloprotease that degrades
242 several proteins, including LpxC. Deletion of FtsH results in toxic accumulation of LPS
243 via increased LpxC stability, which is lethal to the cell (Ogura et al. 1999). The increased
244 number of transposons in *ftsH* in the Δ*yhcB* library suggest that an increase in LpxC
245 stability in this background is less toxic.

246 The bimodal analysis revealed 121 genes that were predicted to be essential in a
247 Δ*yhcB* background. However, this analysis pipeline does not identify the non-essential
248 genes that contribute to fitness: such mutants are viable but either more or less fit.
249 Consequently, when compared to the control library they are represented by higher or
250 lower numbers of sequencing reads, respectively. Therefore we further analysed our data
251 using the tradis_comparison.R script (Barquist et al. 2016). This analysis uses edgeR and
252 measures the fold-change of sequence read depth between a condition and control
253 (Robinson et al. 2009). The 382 genes reported to be essential in both libraries were
254 removed from this analysis. After filtering our data, this method identified 22 genes that,
255 when disrupted, confer a fitness advantage (Fig.5D, blue), and 163 genes that, when
256 disrupted, confer a fitness defect in a Δ*yhcB* mutant (Fig. 5D, red; Table S4; Fold change
257 > 2, Q-value < 0.01). By combining these analyses, we defined synthetically lethal genes

258 as those that are both significantly underrepresented by transposon insertion mutants
259 and that have a >2-fold decrease in reads when compared to the control with a Q-value
260 < 0.01. Altogether 87 genes met these criteria: we consider these genes to be
261 synthetically lethal with *yhcB* and they are discussed below (Fig. 5E).
262
263 ***Identification of pathways important for viability of a* yhcB *mutant***
264 As YhcB interacts directly with components of the elongasome, and is synthetically
265 lethal with *rodZ*, we inspected the list of synthetic lethal genes for additional genes
266 involved in peptidoglycan synthesis, remodelling or recycling. Five genes (*mepM*, *mepS*,
267 *dacA, dapF* and *ldcA*) were identified (Fig. 6A). The genes *mepM* and *mepS* encode two
268 of the three peptidoglycan endopeptidases that cleave the 3-4 *meso*-Dap-D-Ala crosslink
269 and are collectively essential for cell elongation in *E. coli* (Singh et al. 2012). However, a
270 third endopeptidase of this group encoded by *mepH,* was not essential in a Δ*yhcB* mutant
271 (Fig. 6A-B). DapF is an epimerase that catalyses the conversion of L,L-diaminopimelate
272 (LL-DAP) to *meso*-diaminopimelate (*meso*-DAP), which is an integral component of the
273 peptidoglycan stem peptide and the primary residue from which cross-links are formed
274 (Richaud et al. 1987). Sacculi isolated from *dapF* mutants have fewer crosslinks (Mengin-
275 Lecreulx et al. 1988). The DD-carboxypeptidase PBP5, encoded by *dacA*, removes the
276 terminal D-alanine from peptidoglycan pentapeptides (Spratt and Strominger 1976), and
277 is the primary carboxypeptidase under standard laboratory growth conditions (Nelson and
278 Young 2000; Nelson and Young 2001). Finally, the cytosolic LD-carboxypeptidase LdcA
279 participates in the recycling of peptidoglycan turnover products (Fig. 6A). Deletion of *ldcA*
280 results in the lysis of cells during entry into the stationary growth phase due to the
281 accumulation of peptidoglycan crosslinking defects (Templin et al. 1999). From these
282 data, it could be inferred that a Δ*yhcB* mutant cannot survive when additional mutations
283 weaken the integrity of the peptidoglycan layer.

284 To determine whether other cellular processes or pathways are enriched among
285 the genes identified as synthetically lethal with *yhcB,* we used the PANTHER
286 overrepresentation test (Mi et al. 2021). This analysis compares the identified proportion
287 of genes in a given functional category to the expected number of genes in a pathway
288 derived from whole genome data (Table S6). Four processes were identified as
289 functionally enriched among the list of synthetic lethal genes: the 'enterobacterial
290 common antigen (ECA) biosynthetic pathway', 'LPS core biosynthesis', 'cell division', and
291 'response to abiotic stimulus' (Fig. 7A). With the exception of the *tol-pal* system (Fig.
292 S7A), the remaining genes listed within the 'cell division' and 'response to abiotic stimulus'
293 categories did not share overlapping functions and we did not pursue these further.

294 Upon closer inspection of LPS biosynthetic pathways, both the heptosyl
295 transferases WaaC and WaaF, and the entire heptose biosynthetic pathway were
296 synthetically lethal (Fig. 7B-C, Fig. S7B). The WaaP kinase, which phosphorylates the
297 first heptose of the inner core, was also essential in a *yhcB* mutant. Enzymes
298 WaaBGQRY were not essential in a Δ*yhcB* background, but mutants were less fit. In
299 contrast, ligation of the third Kdo moiety by WaaZ was non-essential. The acylation of
300 lipid A by LpxM was also essential in a Δ*yhcB* strain (Fig. 7C). Together these data
301 suggest that LPS stability, whether mediated by Lipid-A hexa-acylation or LPS
302 crosslinking interactions, is important for viability of a Δ*yhcB* strain.

303 Within the locus required for ECA biosynthesis the genes *wecCDEF*, *rffH* and
304 *wzxE* were synthetically lethal with *yhcB*, while disruption to *wecB* and *wecG* suggests
305 these genes were not synthetically lethal but the mutants were sick (Fig. 7D, Fig S7C).
306 There were no significant differences in the insertion frequency within genes *wzzE* and
307 *wecA*. WzzE mediates the length of the ECA chains by determining the number of
308 repeating units (Barr et al. 1999), and WecA catalyses the first committed step in ECA
309 biosynthesis: the transfer of *N*-acetylglucosamine-1-phosphate onto undecaprenyl

310 phosphate (Und-P) to form ECA-lipid I. In short, an ECA-null mutant is viable and mutants
311 with variable ECA lengths are also viable; only mid-pathway blocks are lethal. Mutations
312 that introduce a mid-pathway block in ECA biogenesis are known to cause an aberrant
313 cell morphology (Jorgenson *et al*. 2016), due to accumulation of undecaprenyl-linked
314 ECA-lipid II intermediates creating limited availability of Und-P: a compound of limited
315 abundance that sits at the start of several cell envelope biosynthetic pathways (Jorgenson
316 *et al*. 2016). These observations suggest that the combined defects of *yhcB*-deletion and
317 Und-P sequestration are lethal, and indicate that the availability of Und-P might be limited
318 in a *yhcB* mutant.
319
320 ***Identification of mutations that suppress a* yhcB*-deletion defect***
321 In addition to synthetic lethal interactions, mutations that restore a phenotypic
322 defect, so-called suppressor mutations, can assist in the identification of interconnected
323 cellular pathways (Ogura et al. 1999). We applied TIS to identify, at a whole genome
324 scale, all mutations that can restore tolerance to vancomycin or SDS and EDTA, and
325 therefore suppress a Δ*yhcB* phenotype. First, the Δ*yhcB* mutant library was screened on
326 LB agar supplemented with either SDS and EDTA or vancomycin at concentrations that
327 kill the Δ*yhcB* strain. Transposon mutants of the Δ*yhcB* library able to grow under these
328 conditions were identified as before (Fig. 8A-B). We used the recently published
329 AlbaTraDIS package to analyse our data (Page et al. 2020). We identified 28 gene-
330 deletion suppressor mutations shared between both conditions, and therefore considered
331 these to be universal suppressors (Fig. 8C; Table S7). Of note among the 28 universal
332 suppressors was the Mla pathway. All genes of the pathway have insertions along the full
333 length of each CDS indicating a disruption at any stage of the pathway is restorative to
334 both vancomycin and SDS and EDTA sensitivity (Fig. 8D). This was unexpected as *mla*

335 mutants are highly sensitive to SDS and EDTA (Malinverni and Silhavy 2009; Ekiert et al.
336 2017; Isom et al. 2017).

337 Deletion of *nlpI* was also identified as a universal suppressor (Fig. S8A). NlpI is an
338 OM lipoprotein that functions as an adaptor protein for peptidoglycan endopeptidases
339 (Banzhaf *et al*., 2020) and mediates the degradation of MepS by the protease Prc
340 (Tadokoro et al. 2004; Singh et al. 2015). In a Δ*nlpI* strain, MepS activity is significantly
341 increased (Singh *et al*. 2015), which has been shown to enhance peptidoglycan synthesis
342 by stimulating PBP1B-mediated peptidoglycan synthesis and directing peptidoglycan
343 precursors away from the elongasome complex (Lai et al. 2017), presumably to facilitate
344 the repair of defects in the PG (More et al., 2019). Consistent with this hypothesis, *mrcB*
345 (PBP1B) was identified in the list of genes that confer a fitness defect on a *yhcB* mutant
346 strain when deleted (Table S4), while deletion of *mrcA* (PBP1A) and *lpoA*, which encodes
347 the PBP1A activator, were identified as universal suppressors. Suppressor analysis
348 therefore supported a functional link between YhcB and PG synthesis.

349 Another universal suppressor we identified was deletion of *fabF,* genetically linking
350 *yhcB* with fatty acid biosynthesis (Fig. S8B). FabF, together with FabB, are the two β-
351 ketoacyl-[acyl carrier protein] synthases involved in fatty acid elongation (Garwin et al.
352 1980a). FabB is the major synthase and is essential while FabF is predominantly required
353 at low temperatures to increase membrane fluidity by increasing the proportion of
354 diunsaturated phospholipids (Garwin et al. 1980b), as FabF is more efficient than FabB
355 at elongating palmitoleic acid (16:1Δ9) to cis-vaccinic acid (18:1Δ11). Therefore, loss of
356 *fabF* might result in decreased membrane fluidity or a decreased rate of phospholipid
357 synthesis, or both.

358 We plotted the total suppressor insertion data on a genome map to view relative
359 mutant abundance; the assumption here is that read depth is representative of mutant
360 abundance, which correlates with fitness and is an indicator of the strength of the

361 suppression. In addition to Δ*fabF*, disruption of the *mla* operon and Δ*nlpI* we observed a
362 substantial peak at the *uppS-cdsA* locus in both conditions (Fig. 9A). UppS, encoded by
363 *uppS* (*ispU*), is an undecaprenyl pyrophosphate synthase, which synthesises
364 undecaprenyl diphosphate (Und-PP), the only source of *de novo* synthesised Und-PP
365 and the precursor to Und-P (Apfel et al. 1999; Kato et al. 1999). CdsA sits before the
366 branchpoint in the synthesis of the major phospholipids and catalyses the synthesis of
367 cytidine diphosphate-diacylglycerol from phosphatidic acid (Kanfer and Kennedy 1964;
368 Ganong et al. 1980). Both UppS and CdsA are essential, as such, neither gene can be
369 disrupted by transposon insertion. However, we observed that disruption upstream of the
370 *uppS-cdsA* operon is significant in both suppressor conditions (Fig. 9B). It was unclear
371 from the insertion pattern the effect that disruption at this locus would have. However,
372 these data suggest that deregulation of the native level of expression of *uppS-cdsA* is
373 restorative in a *yhcB* mutant background.

374 Finally, during screening of the transposon mutant library on supplemented agar
375 plates, we also isolated six colonies of the parent Δ*yhcB* strain growing on the control
376 plates of LB supplemented with vancomycin, assumed to be natural revertant
377 suppressors of Δ*yhcB*. The revertant suppression was confirmed by plating on both
378 vancomycin and SDS-EDTA, as well as confirming gene-deletion by PCR of the *yhcB*
379 locus (Fig. S9A-B). We sequenced the genomes of these isolates and identified the
380 mutations listed in Table S8. Two isolates contained either the reported *mlaA** mutation
381 or a variation of this mutation (mut4 and mut6), while one isolate had a genome inversion
382 that resulted in separation of the *mla* operon from its promoter region (mut2). The *mla*
383 inversion mutation restored resistance to both vancomycin and SDS-EDTA, consistent
384 with the earlier TIS data, but did not fully restore cell size (Fig. S9A-C). The *mlaA**
385 mutation is well characterised and is toxic in a WT background as it results in LPS
386 overproduction as a consequence of increased LpxC stability (May and Silhavy 2018).

387 However, these mutations are not toxic in a Δ*yhcB* mutant and restore cell size and
388 resistance to vancomycin (Fig. S9A-C). We also identified a single nucleotide
389 polymorphism (SNP) in *lpxC* that restored resistance to vancomycin and SDS-EDTA but
390 did not restore cell size (mut1). These data are suggestive of either a defect in LPS
391 synthesis or export, or an imbalance in LPS to phospholipid at the outer membrane of a
392 Δ*yhcB* mutant, rendering the *mlaA** mutation non-lethal in this background.

393 Finally, two isolates each had a SNP that resulted in a single amino acid
394 substitution in CdsA. We used Phyre2 to predict the structure of CdsA (Kelley et al. 2015).
395 The predicted structure was very similar to the experimentally determined structure of
396 CdsA, derived from *Thermotaga maritama*, with an RMSD value of 0.404 Å (Fig. S9D)
397 (Liu et al. 2014). The active site of CdsA is a conserved, negatively charged pocket
398 occupied by two cation cofactors that are critical for function (Fig. S9D). Mutations within
399 this region that hinder cation binding result in decreased enzyme activity (Liu et al. 2014).
400 The mutations identified within CdsA in our revertant suppressor mutants (S231L and
401 S239G, respectively) each result in substitution of a serine residue proximal to the metal
402 ion binding site (Fig. S9D). A mutation of S223C in *T. maritama* CdsA, which corresponds
403 with residue S239 in *E. coli*, results in severely reduced CdsA function (Liu et al. 2014).
404 The two mutations within CdsA in the revertant suppressor mutants likely result in
405 decreased function of CdsA. Both mutants with a SNP in CdsA (mut3 and mut5) restored
406 resistance to both vancomycin and SDS and EDTA, in addition to cell size (Fig. S10A-C).
407

408 ***Characterisation of a* yhcB*-mutant envelope***

409 Our genetic screening revealed a connection with phospholipid biosynthesis (*fabF,*
410 *cdsA*) and trafficking (*mla*), Previous research has shown that fatty acid availability
411 determines the cell size via phospholipid biosynthesis (Vadia et al. 2017). Increased
412 phospholipid production resulted in a larger cell size that was reminiscent of a Δ*yhcB*

413 mutant (Vadia et al. 2017). As such, we hypothesised that phospholipid production might
414 be increased in a *yhcB* mutant. We first investigated whether membrane "lipid ruffles"
415 resulting from increased phospholipid synthesis, and resembling those reported by Vadia
416 et al. (2017), could be detected in a *yhcB* mutant. Following 3 hours of growth in LB, *E.*
417 *coli* BW25113 and an isogenic *yhcB* mutant were stained with MitoTracker to label
418 internal lipid structures (Vadia et al. 2017). Microscopic evaluation of these cells revealed
419 that *E. coli* BW25113 membranes stained uniformly. In contrast, intensely stained spots
420 indicative of accumulation of lipid structures were observed in the *yhcB* mutant (Fig.
421 S10A). Subsequent imaging of cells by transmission electron microscopy confirmed the
422 aberrant size of *yhcB* mutant cells and revealed the presence of excess membrane
423 structures (Fig. 10A, Fig. S10).

424 Given the increase in phospholipid biogenesis noted above we next investigated
425 the composition of phospholipids species. We extracted the total phospholipid species
426 using the Bligh and Dyer method (Bligh and Dyer 1959), and separated these by thin
427 layer chromatography (Matsumoto et al. 1998). The phospholipid composition of *E. coli*
428 is approximately 75% phosphatidyl ethanolamine, 20% phosphatidyl glycerol and 5%
429 cardiolipin with lysophospholipids typically making up <1% of total phospholipid species
430 (Rowlett et al. 2017; Zheng et al. 2017). The relative ratios of phosphatidylethanolamine,
431 phosphatidylglycerol and cardiolipin were similar in the parent and Δ*yhcB* strains.
432 However, during growth in LB, we observed an additional phospholipid species that was
433 present in both strains, but only the Δ*yhcB* mutant strain in stationary phase (Fig.10B and
434 S10B). This was not observed when the mutant was grown in M9-glucose (Fig. S10C).
435 By using known lipid standards, the additional spot in the Δ*yhcB* mutant stationary phase
436 was identified as most likely lysophosphatidylethanolamine (LPE; Fig. 10B).

437 LPE can be derived from PE hydrolysis or lipoprotein maturation. However, in a
438 cell with a stressed envelope, the primary source of LPE accumulation occurs via PE

439 hydrolysis (Zheng et al. 2017). Two OM proteins, PldA and PagP, maintain the OM
440 asymmetry by cleaving phospholipids that accumulate in the outer leaflet of the OM. PldA
441 degrades phospholipids while PagP, a Lipid A palmitoyltransferase, cleaves an acyl chain
442 from PE and catalyses its transfer to Lipid A resulting in hepta-acylated LPS (Bishop et
443 al. 2000). Both reactions result in an increase in free LPE. As PagP is usually inactive in
444 the OM and activity is stimulated in response to migration of phospholipids into the outer
445 leaflet (Jia et al. 2004), measuring the amount of hepta-acylated LPS is an established
446 proxy for detecting loss of OM asymmetry (Chong et al. 2015). We quantified the amount
447 of hepta-acylated lipid A relative to hexa-acylated lipid A and identified a significant
448 increase in hepta-acylated lipid A in the Δ*yhcB* mutant compared to the WT; a phenotype
449 that is exacerbated by prolonged growth (Fig. 10C). Together these data suggest that
450 excess phospholipid production in a *yhcB* mutant background results in an increase in
451 cell size and loss of OM asymmetry, resulting in hepta-acylation of lipid A and
452 accumulation of LPE.

453 Cell membrane synthesis must be coordinated with peptidoglycan biogenesis to
454 maintain cell envelope integrity. As the peptidoglycan layer defines cellular morphology,
455 and we had observed a swollen morphology of *yhcB* mutants, we hypothesised that the
456 peptidoglycan layer of a *yhcB* mutant may be compromised. Indeed, our genetic evidence
457 supports the hypothesis that mutations (*dapF, dacA*) that weaken integrity of the
458 peptidoglycan are lethal. We therefore analysed the muropeptide composition of the cell
459 wall. Cells were grown in LB and collected at both exponential and stationary phase.
460 Peptidoglycan was purified and digested by the muramidase cellosyl, and the resulting
461 muropeptides were analysed by HPLC (Glauner 1988). There were no significant
462 differences in the muropeptide species identified (Fig S11; Table S5). However, we did
463 identify differences in the amount of crosslinking between strains and growth phases (Fig.
464 10D). While the degree of peptidoglycan crosslinking in the WT strain was increased in

465 stationary phase compared to exponential phase, consistent with the literature (Templin
466 et al. 1999), this same transition was not observed in the *yhcB* mutant, suggesting either
467 a limitation in the rate of peptidoglycan crosslinking or an increased rate of crosslinking
468 hydrolysis in a *yhcB* mutant. The muropeptide analysis, together with the phospholipid
469 analysis, support our finding that a *yhcB* mutant is unable to sustain rapid exponential
470 growth and indicate a defect in the ability to transition into stationary phase.

471 In addition to a synthetically lethal relationship with genes involved in
472 peptidoglycan assembly, recycling and remodelling (*mepS, mepM, ldcA, nlpI*) our TIS
473 data also indicated that mutations in the ECA biosynthetic pathway that sequester
474 undecaprenol phosphate (Und-P) are lethal in a *yhcB* mutant. We hypothesised that the
475 availability of Und-P might be limited in a Δ*yhcB* mutant, affecting peptidoglycan synthesis
476 (Danese *et al*. 1998; Ramos-Morales *et al*. 2003; Jorgenson *et al*. 2016). In addition to
477 peptidoglycan and ECA biosynthesis, Und-P is also a lipid carrier for O-antigen, however,
478 most *E. coli* K-12 strains, including BW25113, do not have O-antigen as a result of an
479 insertion element in *wbbL* (Liu and Reeves 1994). Therefore, to investigate whether
480 sequestration of Und-P is toxic to a *yhcB* mutant, we tried to restore O-antigen. The
481 transformation efficiency of the *yhcB* mutant with *wbbL* to restore O-antigen was strikingly
482 reduced, suggesting that Und-P limitation is lethal to a *yhcB* mutant (Fig. S10D). One
483 mechanism to suppress Und-P limitation is to upregulate expression of *uppS,* the gene
484 required for Und-P synthesis. Indeed, our TIS data reveal insertions that suppress the
485 *yhcB* phenotype in the promoter region to *uppS*. Furthermore, complementation of a *yhcB*
486 mutant with ectopically expressed *uppS*, but not *cdsA,* suppressed both the vancomycin
487 and SDS-EDTA sensitivity defect of a *yhcB* mutant (Fig. 10E).

488 During our analysis we noted that *uppS* and *cdsA* are highly co-conserved across
489 the bacterial kingdom (Fig. S12) and share a conserved operon structure in many
490 bacterial phyla (Fig.S13) (Saha et al. 2020). We hypothesise that the upregulation of

491 *uppS* would result in increased expression of *cdsA*, and in turn give rise to excess
492 phospholipid synthesis. This hypothesis is supported by our finding that loss of function
493 mutations in the metal-binding pocket of CdsA restore all *yhcB* defective phenotypes (Fig.
494 9C).
495

496 **Discussion**

497 Here we have applied a high-density mutagenesis screen to comprehensively map
498 the genetic interactions of a single gene, *yhcB*. With thousands of deleterious and
499 restorative genetic interactions discovered, to the best of our knowledge no other gene
500 has been scrutinised genetically at such scale and resolution. Our data reveal that a
501 Δ*yhcB* mutant has a cell envelope permeability defect, dysregulated cell size, and
502 epistatic interactions with multiple pathways of cell envelope biogenesis. The defect
503 introduced by deletion of *yhcB* is most severe during rapid growth in rich media, when the
504 demand for synthesis of cell envelope material is greatest. In addition, toxicity progresses
505 with sustained growth in rich medium, with a decrease in cell viability observed upon
506 transition to stationary phase, a period of growth when *de novo* synthesis machineries
507 are switched off. Taken together, these observations indicate that a *yhcB* mutant is either
508 limited in the ability to recycle existing components of the envelope during synthesis, or
509 limited in *de novo* synthesis of one or more cell envelope components. This hypothesis
510 is supported by the cell growth model put forward by Harris and Theriot (2016) that when
511 cell envelope synthesis is impeded, an increase in cell width is observed decreasing the
512 surface area to cell volume ratio and enabling the same amount of cell volume to be
513 encapsulated by less material.

514 The pathways for synthesis of the different components of the Gram-negative cell
515 envelope are intrinsically linked: they share several common precursors and tightly
516 interconnected feedback mechanisms (Fig. 11A). If the rate of peptidoglycan biosynthesis

517 is decreased, the rate of LPS biosynthesis needs to be decreased accordingly to avoid
518 the toxic effects of LPS accumulation (Sullivan and Donachie 1984; May and Silhavy
519 2018). Moreover, a recent paper identified that deletion of the *mla* pathway confers a
520 fitness advantage in cells exposed to fosfomcin, a MurA inhibitor, connecting decreased
521 PG synthesis with a requirement for decreased PL trafficking (Turner et al. 2020).
522 Similarly, when LptC, a component of the LPS export system, is depleted the relative
523 abundance of proteins involved in phospholipid biosynthesis and trafficking are also
524 depleted indicating a feedback mechanism that couples phospholipid synthesis and
525 export with LPS demand (Martorana et al. 2014). In a *yhcB* mutant we observed
526 weakened peptidoglycan integrity and a loss of OM asymmetry, coupled with an increase
527 in cell size and internal phospholipid membrane structures (Fig. 11B). These findings
528 connect YhcB with every layer of the cell envelope.

529 Our observations of excess phospholipid membranes and an increased cell size
530 in a *yhcB* mutant resemble the phenotype reported by Vadia *et al.* (2017) that results from
531 increased phospholipid synthesis. We hypothesise that the increase in phospholipid
532 production results in loss of OM asymmetry, with substantial amounts of phospholipid
533 integrating into the outer leaflet of the OM to compromise the barrier function of the cell
534 envelope. This hypothesis is supported by several lines of evidence. First inhibition of
535 phospholipid synthesis by mutations within the metal ion binding site of CdsA, or loss of
536 FabF, which regulates membrane fluidity, are restorative to a *yhcB* mutant. Furthermore,
537 treatment with sub-inhibitory concentrations of cerulenin, an antibiotic that targets the
538 FabB and FabF elongation step of fatty acid synthesis, is beneficial to growth of a *yhcB*
539 mutant (Nichols et al. 2011). Second, a *mlaA** mutation, which increases mislocalisation
540 of phospholipids at the OM triggering subsequent phospholipid degradation by PldA and
541 is toxic in a wild-type background, is tolerated in a *yhcB* mutant, restores cell size, and
542 re-establishes the barrier function of the OM. Third, an increase in LPS production

543 through the loss of the essential protease FtsH, the introduction of *mlaA** which
544 upregulates LpxC production, or by mutation of its target LpxC can be tolerated. Overall,
545 mutations that result in a decrease of phospholipid biosynthesis and trafficking, or an
546 increase in LPS biosynthesis are restorative, indicative of an underlying imbalance in PL
547 to LPS levels.

548 We found that mutations that weaken PG integrity are lethal in a *yhcB* mutant
549 indicating that the rate of PG synthesis is also not coordinated with cell expansion. While
550 the composition of the PG in a *yhcB* mutant resembles that of the WT, our data reveal
551 that loss of PG synthesis by the elongasome is restorative. In contrast, loss of PG
552 synthesis by the divisome had a negative effect while mutations that stimulate PG
553 synthesis via the divisome are restorative. Given the location of YhcB and the phenotypes
554 of a deletion mutant, an attractive hypothesis is that YhcB is involved in switching PG
555 synthesis between the elongasome and divisome. In support of this hypothesis a recent
556 paper reported the interaction and co-purification of YhcB with proteins of the divisome
557 (Mehla et al. 2021).

558 Another attractive hypothesis is that YhcB has a role in sensing the availability of
559 Und-P, or recycling/synthesis of Und-P. This latter hypothesis is supported by several
560 observations. First, mutations in the ECA biosynthesis pathway that sequester Und-P and
561 limit the available pool are lethal. Second, restoration of WbbL activity is toxic in a *yhcB*
562 mutant, suggesting that Und-P availability is limited. Third, a *yhcB* mutant is reported to
563 be more sensitive to bacitracin (Nichols et al. 2011), which targets BacA. BacA is
564 responsible for recycling approximately three quarters of Und-PP back to Und-P following
565 release of its substrate in the periplasm. Fourth, deletion of *mrcB* in cells with low levels
566 of Und-P results in heterogenous cell lysis, and *mrcB* was identified in the list genes in
567 which an epistatic interaction with *yhcB* causes a fitness defect. These data are
568 consistent with the finding that only a sub-population of the Und-P depleted *mrcB* mutants

569 lyse (Jorgenson et al. 2019). Lastly, upregulation of *uppS*, but not *cdsA*, was universally
570 restorative in a *yhcB* mutant.

571 The observation that the *uppS-cdsA* operon structure is conserved across bacteria
572 reveals the tight linkage between phospholipid production and the synthesis of
573 polysaccharide components of the cell envelope. The observation that cell size,
574 resistance to vancomycin, and resistance to SDS-EDTA can be decoupled in suppressor
575 screens indicate that YhcB interacts with multiple cell envelope biogenesis pathways.
576 Indeed, in addition to forming a dimer and reports of larger homo-multimer structures
577 (Maddalo et al. 2011; Li et al. 2012; Mehla et al. 2021), YhcB is known to interact with
578 several components of the elongasome (Li et al. 2012), and has also been identified as
579 an interaction partner of LapA (Hu et al. 2009; Li et al. 2012). LapA (YciS) forms a
580 complex with LapB (YciM), FtsH and YejM to regulate LpxC stability and thus LPS
581 abundance (Clairfeuille et al. 2020; Fivenson and Bernhardt 2020; Guest et al. 2020).
582 The role of LapA is unclear but deletion of *lapA* results in minor accumulation of
583 incomplete LPS precursors (Klein et al. 2014). The interaction of YhcB with the
584 elongasome and the LpxC regulation complex via LapA positions YhcB at the interface
585 between two of the major complexes that coordinate envelope synthesis (Fig. 11C). This
586 hypothesis is supported by the observation that deletion of different YhcB domains gives
587 rise to different chemical sensitivity profiles.

588 In conclusion, YhcB plays an important regulatory function at the interface between
589 all of the cell envelope biogenesis pathways, and this function is mediated by physical
590 interactions between members of the elongasome and LPS regulation systems. While
591 the precise molecular events facilitating the regulation of these pathways has yet to be
592 elucidated, as *yhcB* is conserved among Gammaproteobacteria, is required for tolerance
593 to polymyxin B, colistin, and vancomycin, and is necessary for the colonisation of different

594 hosts (Harvey et al. 2011; Brooks et al. 2014; Jana et al. 2017), it provides a novel
595 antimicrobial target for exploitation against clinically important pathogens.
596
597 **Materials and Methods**
598 *Strains, media and growth conditions*
599 The parent strain for this work was *E. coli* K-12 strain BW25113. Gene deletion mutants
600 were constructed by P1 transduction and using the Keio library strains as donors (Baba
601 et al. 2006; Thomason et al. 2007). The kanamycin cassette was removed using the
602 pCP20 vector (Datsenko and Wanner 2000). The mutant was confirmed by PCR and
603 Sanger sequencing. Bacteria were grown in Luria-Bertani (LB: 10 g tryptone, 5 g yeast
604 extract, 10 g NaCl) medium or on LB plates (LB supplemented with 1.5% nutrient agar)
605 and incubated at 37°C. When required, media were supplemented with 50 µg/ml
606 kanamycin or 100 µg/ml carbenicillin. The M9-glucose recipe used was: 1x M9 salts
607 (Sigma Aldrich), 200 µl filter sterilised 1 M $MgSO_4$, 10 µl filter sterilised 1 M $CaCl_2$, and 2
608 ml of either a 20% (w/v) D-glucose or 20% (v/v) glycerol solution per 100 ml. For micro-
609 dilution spot plates, unless otherwise stated, bacteria were grown overnight in 5 ml LB
610 medium at 37°C with aeration. Cultures were normalised by optical density to an OD_{600}
611 of 1.00, 10-fold serially diluted in LB, and 2 µl of each dilution was inoculated onto LB
612 agar plates.
613
614 *Complementation assays*
615 The BW25113 and *yhcB* strains were transformed with a pBAD-Myc-His-A plasmid with
616 and without the *yhcB* coding sequence under the control of the arabinose promoter. O-
617 antigen was restored as described previously (Browning et al. 2013). In brief, cells were
618 transformed with a pET20b plasmid DNA encoding *wbbL* Additional copies of *cdsA* and

619 *uppS* were introduced, independently, on a pASK-IBA2C plasmid under the control of a
620 tetracyclin-inducible promoter.
621
622 *Polymyxin B TIS screen*
623 An amended version of the Andrews broth microdilution protocol in 96-well plate format,
624 adjusting the starting inoculum to an initial OD_{600} of 0.05 and the growth medium to LB,
625 was used to identify an initial inhibitory concentration range or polymyxin B (Andrews
626 2001). Growth curve experiments of *E. coli* BW25113 were then repeated in 50 ml LB
627 supplemented with polymyxin B in glass flasks, reflecting the conditions of the TIS screen.
628 A concentration of 0.2 µg/ml polymyxin B was identified as sub-inhibitory for growht of
629 BW25113. The transposon library was inoculated into 50 ml LB medium with and without
630 0.2 µg/ml polymyxin B (Sigma Aldrich), in duplicate, at a starting optical density of 0.05,
631 equivalent to a copy number of ~2,500 of each mutant, and grown to OD_{600} = 1.00, at
632 37˚C with aeration. Cells were harvested, and genomic DNA prepared for sequencing.
633 As we knew the density of this library (Goodall et al. 2018), we estimated the number of
634 mapped reads, and therefore sequencing coverage, needed to ensure sufficient sampling
635 of the library using the equation $\mathrm{I} = s - s(\frac{s-1}{s})^n$, where I = insertions, and n = number of
636 mapped reads (Fig. S1B). For a theoretical library of 1 million mutants, assuming no loss
637 of mutants and an equal chance of each transposon junction being sampled, ~2.3M reads
638 are needed to ensure sampling of 90% of the library, with diminishing returns with further
639 sequencing. Obtaining >4.2 M reads should enable sampling of 99% of the possible
640 unique insertion sites. Therefore, we collected >2 M sequencing reads per replicate, and
641 a combined total of >4.2 M reads per condition, to give us confidence that any observed
642 loss of mutants is not due to insufficient sampling.
643
644 *Microscopy*

645 Samples were taken directly from overnight cultures grown at 37˚C in their respective
646 media for 16 h and diluted to an OD_{600} of 0.10. 5 µl cells were spread on a 1 mm glass
647 slide pre-treated with 5 µl poly-L-lysine (Sigma Aldrich). A Nikon 90i eclipse microscope
648 was used to capture differential interference contrast (DIC) images of cells, using a 40x
649 objective lens with a Nikon immersion oil. These images were collected at the University
650 of Birmingham. Cell dimensions were measured using ImageJ (Schindelin et al. 2012).
651 Fluorescent labelling of lipids was previously described by Vadia *et al*. (2017). These
652 experiments were done at the University of Queensland. M9-glucose overnight cultures
653 were diluted into fresh LB medium and after 2 h of growth at 37˚C, 0.2 µM MitoTracker®
654 Green FM (Invitrogen) was added to each sample to label lipids. After incubation for a
655 further 1 h, bacteria from 1 ml samples were harvested by centrifugation and
656 resuspended in 500 µL of FM™ 4-64FX (Invitrogen) at 5 µg/mL, to label *E. coli*
657 membranes, and incubated for 5 min at room temperature. Bacteria were embedded on
658 1% agarose pads and imaged using a confocal microscope Inverted LSM 880 Fast
659 Airyscan (63x/1.40 OIL). Electron microscopy was performed at the University of
660 Queensland. Conventional fixation and embedding in resin was undertaken using a
661 protocol adapted from (Fassel et al. 1997). Briefly, bacteria were applied to dishes with
662 glass coverslips coated in poly-L-lysine and then fixed in 2% PFA, 2.5% Glutaraldehyde,
663 and 0.075% Ruthenium Red. Samples were then washed 3x10min in PBS and postfixed
664 in 1% osmium, then again in 1% osmium with 3% potassium ferricyanide. Bacteria
665 underwent serial dehydration in increasing concentrations of ethanol and were then
666 infiltrated and embedded with Epon resin. Fast freezing and freeze substitution of bacteria
667 was undertaken as described previously (Ariotti et al. 2012; Walser et al. 2012). Briefly,
668 bacteria were applied to carbon-coated poly-L-lysine treated sapphire discs and frozen in
669 a Leica EMPACT 2 high pressure freezer. They were then freeze substituted in a EM
670 AFS 2 system (Leica Microsystems GmbH, Wetzlar, Germany) and embedded into Epon

671 resin. Ultra-thin sections were obtained using a Leica Ultracut UC6 Ultramicrotome and
672 micrographs acquired on a JEOL 1011 transmission electron microscope equipped with
673 a Morada CCD camera.
674
675 *Phospholipid extraction*
676 Total phospholipids were extracted using an amended version of the Bligh-Dyer method
677 (Bligh and Dyer 1959). 10 ml of culture at an OD_{600} ~ 4.00, or 100 ml of culture at an
678 OD_{600} of 0.40 was centrifuged at 4˚C to harvest cells. The supernatant was discarded,
679 and pellet resuspended in 1 ml ddH_2O and transferred to a glass tube. 1.25 ml chloroform
680 and 2.5 ml methanol were added to the sample using glass pipettes. The sample was
681 vortexed for 20 s to create a single-phase solution which was then incubated at 50°C for
682 30 min. A further 1.25 ml chloroform and 1.25 ml water was added to the sample to create
683 a 2-phase solution and incubated again at 50°C for 30 min. The sample was centrifuged
684 at 400 x *g* for 10 min at RT and the lower organic phase containing phospholipids was
685 transferred to a new glass tube using a glass Pasteur pipette. Chloroform was
686 evaporated by placing the glass tubes in a heat block at 50°C under a stream of nitrogen.
687
688 *Thin Layer Chromatography*
689 10 µl of sample was spotted onto the origin of a TLC silica gel membrane (Merck) using
690 a 5 µl glass capillary tube (Sigma Aldrich). Once dry, the membrane was transferred to
691 an equilibrated solvent system of 65:25:4 chloroform:methanol:water (Matsumoto et al.
692 1998). The samples were separated until the solvent front had migrated sufficiently from
693 the origin then the membrane was removed from the solvent tank and was air dried at
694 RT. Samples were stained with phosphomolybdic acid (PMA) 10% solution in ethanol
695 and heated with a heat gun to activate the PMA until lipid species were visible. Lipid

696 standards were purchased from Avanti Polar Lipids and handled according to
697 manufacturer instructions.
698
699 *Lipid A palmitoylation assay*
700 Lipid A labelling, extraction and analysis were done as described and demonstrated
701 previously (Chong et al. 2015). As a positive control, BW25113 was exposed to 25 mM
702 EDTA for 10 min to induce PagP mediated palmitoylation of Lipid A, before harvesting
703 cells by centrifugation.
704
705 *Peptidoglycan extraction and analysis*
706 Cell cultures were grown in LB medium at 37˚C and harvested at an OD of 0.4 and 4.00,
707 in triplicate. After pelleting the cells and resuspending in ice-cold water, the cell
708 suspension was dropped into 8% boiling SDS solution. Peptidoglycan was purified, and
709 muropeptides were released with cellosyl and analysed by HPLC as described (Glauner
710 1988).
711
712 *Construction of transposon-mutant libraries*
713 10 ml of 2x TY broth was inoculated with a single colony and grown overnight at 37°C
714 with aeration. The 10 ml overnight culture was used to inoculate 800 ml 2x TY broth in a
715 2 L flask and grown at 37°C with aeration until OD_{600} 0.6-0.9. At the desired OD, cells
716 were collected and stored on ice for 30 min before centrifugation to pellet the cells.
717 Electrocompetent cells were prepared by repeatedly centrifuging cells and resuspending
718 in decreasing amounts of ice-cold 10% (v/v) glycerol. The final resuspension was in 1 ml
719 of 10% glycerol resulting in a dense ~2 ml cell culture. Aliquots of 200 μl cells were
720 distributed between 1.5 ml microcentrifuge tubes. 0.2 μl EZ-Tn5™ transposome (Epibio)
721 was mixed with each aliquot of cells and incubated on ice for 30 min. Samples were

722 transferred to pre-chilled 2 mm gap electroporation cuvettes (Cell Projects Ltd.). Cells
723 were pulsed at 2200 V and 2 ml of pre-warmed SOC medium was immediately added to
724 the sample for recovery. Samples were transferred to a 15 ml falcon tube to allow for
725 maximum aeration and were incubated at 37°C for 2 h. 5 ml of LB broth was added to
726 each 15 ml falcon tube. ~4-5 drops of cells (equivalent to ~200 μl) were spread per LB
727 agar plate supplemented with 50 μg/ml kanamycin. Sufficient cells were inoculated per
728 plate to form non-touching single colonies. Plates were incubated overnight at 37°C for
729 18 h. Following incubation, 500 μl 30% glycerol-LB broth was added to each plate and
730 using a 'hockey-stick' spreader, colonies were scraped off the surface of the agar plate
731 and pooled. Cells were mixed thoroughly before storing at -80°C.
732
733 *Screening of the* yhcB *transposon-mutant library to identify suppressor mutations*
734 Cell cultures were resuspended in 1 ml of OD_{600} = 1.00, 200 µl of culture was plated
735 across 5x LB agar plates with or without additional chemical stresses. Assuming a library
736 of ~500,000 mutants (as judged from the unique insertions), this number of cells equates
737 to approximately 2,000 independent copies of each individual transposon mutant. We
738 chose a plate-based screening method as this minimises competition between mutants,
739 allowing for identification of slow growing mutants in addition to strong suppressor
740 mutations. Cultures were diluted to such quantities that single colonies of transposon
741 mutants could be isolated on the plates supplemented with stresses to prevent the growth
742 of satellite colonies and therefore false positive results. Plates were incubated at 37˚C for
743 24 h. Colonies were scraped and pooled for sequencing.
744
745 *TIS sequencing*
746 Genomic DNA (gDNA) was extracted and quantified using Qubit™ dsDNA HS Assay kit
747 (Invitrogen). 1 µg of gDNA was fragmented by mechanical shearing using a bioruptor

748 (Diagenode) using the shearing profile 30 s ON, 90 s OFF at low intensity, resulting in
749 DNA fragments with an average length of ~300 bp. Fragmented DNA was end-repaired
750 using the NEBNext Ultra I kit (New England Biolabs). The fragments were then ligated
751 with an adapter, and the sample was purified in a size-selection step using AMPure XP
752 SPRI beads (Beckman Coulter) before transposon-junctions were enriched by PCR with
753 primers specific for the transposon and the adapter. The Transposon-gDNA junctions
754 were prepared for sequencing by PCR addition of Illumina adapters using the NEBNext
755 Multiplex Oligos for Illumina (New England Biolabs). However, the forward Universal
756 primer was replaced with custom primers that include the Universal primer sequence
757 followed by a 6-9 nucleotide barcode (to introduce complexity and stagger the start of the
758 transposon sequence) and a 22 nt sequence with homology to the transposon at the 3′
759 end of the primer. Samples were purified after each PCR step using SPRI beads at a
760 ratio of 0.9:1 beads to sample. Finally, the sample was quantified using the KAPA Library
761 Quant Kit (Illumina) Universal qPCR Mix (Kapa Biosystems). Samples were pooled,
762 denatured and diluted to 18 pM and sequenced using an Illumina MiSeq, with 5% (v/v)
763 20 pM PhiX (Illumina), using 150 cycle v3 cartridges. Data are available at the European
764 Nucleotide Archive (accession: PRJEB43420).
765
766 *TIS analysis*
767 Data were first demultiplexed using the Fastx barcode splitter, to remove the 5′ end
768 barcode (inline index) unique to each sample (Pearson et al. 1997). The BioTraDIS
769 analysis package (version 1.4.5) was used for the remaining data processing (Barquist
770 et al. 2016). We allow for up to 4 bp mismatches in the transposon pattern matching step.
771 When successfully identified transposon sequences have been identified, the transposon
772 is trimmed and the remaining read is mapped to the BW25113 reference genome using
773 bwa (accession CP009273.1) to generate insertion plot files. These data can be viewed

774 online at our browser: http://tradis-vault.qfab.org/. The plot files are input to the
775 tradis_gene_insert_sites script to calculate the number of insertions per gene (insertion
776 index score). Unless otherwise stated, 5% trim was applied to both the 5′ and 3′ end of
777 each gene. The tradis_essentiality.R script was used to calculate the probability of
778 belonging to each mode representing essential and non-essential gene populations
779 respectively. The tradis_comparison.R script was used to compare read depth between
780 control and condition samples, per gene, using a threshold of >2-fold change and a Q-
781 value < 0.01. Plot files generated by the BioTraDIS analysis were also used as inputs for
782 AlbaTraDIS. AlbaTraDIS (version 1.0.1) was used for comparative analysis between
783 suppressor TIS datasets (Page et al. 2020). The reference genome annotation was used
784 to define gene boundaries. We set the minimum log counts per million threshold at 10,
785 for all other settings the default conditions were used.
786
787 *Whole genome sequencing*
788 Whole genome sequencing was done by MicrobesNG, University of Birmingham, UK,
789 using Illumina platforms generating short read data. Sequencing data were aligned to the
790 *E. coli* BW25113 reference genome available from the NCBI database (CP009273.1)
791 using bwa mem and then converted to bam files and sorted and indexed using SAMtools
792 (Li et al. 2009; Langmead and Salzberg 2012). Data are available at the European
793 Nucleotide Archive (accession: PRJEB43420). The programs Snippy and VarScan were
794 used to identify SNPs and indels, BreSeq was used to identify large chromosomal
795 rearrangement events (Koboldt *et al*. 2012; Deatherage & Barrick 2014; Seeman 2015).
796
797 *Phylogenetic analysis*
798 All searches were performed against the UniProt database of Reference Proteomes
799 (v2020_06, 02-Dec-2020), which includes only complete proteomes of reference

800 organisms, to confidently determine presence as well as absence. Search was performed
801 with PF06295.13 using hmmsearch (3.1b2; (Eddy 2011)) with the --max setting. Search
802 results were analysed manually as well as by all-against-all blast and subsequent
803 clustering in cytoscape, to determine the search cutoff used. Taxonomy information was
804 equally obtained from the UniProt Reference Proteomes ftp site (v2020_06, 02-Dec-
805 2020). Phylogenetic inference was performed on the sequences aligned via mafft (Katoh
806 and Standley 2013), and tree calculation using IQ-TREE (Nguyen et al. 2015) with the
807 built-in model test (Kalyaanamoorthy et al. 2017), which resulted in LG+G4. Tree
808 visualisation was performed using iTol (https://doi.org/10.1093/nar/gkz239).
809

810 **Acknowledgements**

811 We thank Dr. Eugenio Sanchez-Moran at UoB for use of his microscope, and we thank
812 the University of Queensland Microscopy department at the Institute of Molecular
813 Biosciences for assistance in setting up the lipid-labelling microscopy experiments. In
814 particular, thank you Dr. Nicholas Condon for your time and teaching. We thank
815 MicrobesNG for providing a fantastic service generating WGS data, especially Dr. Emily
816 Richardson for patience and sharing your expertise.
817 This research was supported by the Midlands Integrative Biosciences Training
818 Partnership (MIBTIP, BBSRC) Ph.D. program who sponsored E.G. This project received
819 funding from the European Union's Horizon 2020 research and innovation programme
820 under the Marie Skłodowska-Curie grant agreement No 721484 awarded to WV and IRH.
821 B.Z. was supported by a CSC-UQ PhD Scholarship (China Scholarship Council). This
822 work was also supported by the National Health and Medical Research Council of
823 Australia (grants APP1140064 and APP1150083 and fellowship APP1156489 to R.G.P.).
824 RGP is supported by the Australian Research Council (ARC) Centre of Excellence in
825 Convergent Bio-Nano Science and Technology CE140100036. The authors

826 acknowledge the use of the Microscopy Australia Research Facility at the Centre for
827 Microscopy and Microanalysis at The University of Queensland. Microscopy was
828 performed at the Australian Cancer Research Foundation (ACRF)/Institute for Molecular
829 Bioscience Cancer Biology Imaging Facility, which was established with the support of
830 the ACRF.

References

Abellón-Ruiz, J., S. S. Kaptan, A. Baslé, B. Claudi, D. Bumann, U. Kleinekathöfer, and B. van den Berg. 2017. Structural basis for maintenance of bacterial outer membrane lipid asymmetry. *Nature Microbiology* 2: 1616–1623. doi:10.1038/s41564-017-0046-x.

Andrews, J. M. 2001. Determination of minimum inhibitory concentrations. *The Journal of antimicrobial chemotherapy* 48 Suppl 1: 5–16.

Apfel, C. M., B. Takács, M. Fountoulakis, M. Stieger, and W. Keck. 1999. Use of genomics to identify bacterial undecaprenyl pyrophosphate synthetase: Cloning, expression, and characterization of the essential *uppS* gene. *Journal of Bacteriology* 181. American Society for Microbiology: 483–492. doi:10.1128/jb.181.2.483-492.1999.

Ariotti, N., S. Murphy, N. A. Hamilton, L. Wu, K. Green, N. L. Schieber, P. Li, S. Martin, et al. 2012. Postlipolytic insulin-dependent remodeling of micro lipid droplets in adipocytes. *Molecular Biology of the Cell* 23. American Society for Cell Biology: 1826–1837. doi:10.1091/mbc.E11-10-0847.

Ashkenazy, H., S. Abadi, E. Martz, O. Chay, I. Mayrose, T. Pupko, and N. Ben-Tal. 2016. ConSurf 2016: an improved methodology to estimate and visualize evolutionary conservation in macromolecules. *Nucleic acids research* 44. Oxford University Press: W344-50. doi:10.1093/nar/gkw408.

Baba, T., T. Ara, M. Hasegawa, Y. Takai, Y. Okumura, M. Baba, K. a Datsenko, M. Tomita, et al. 2006. Construction of *Escherichia coli* K-12 in-frame, single-gene knockout mutants: the Keio collection. *Molecular systems biology* 2: 2006.0008. doi:10.1038/msb4100050.

Barquist, L., M. Mayho, C. Cummins, A. K. Cain, C. J. Boinett, A. J. Page, G. C. Langridge, M. A. Quail, et al. 2016. The TraDIS toolkit: Sequencing and analysis for dense transposon mutant libraries. *Bioinformatics* 32. doi:10.1093/bioinformatics/btw022.

Barr, K., J. Klena, and P. D. Rick. 1999. The modality of enterobacterial common antigen polysaccharide chain lengths is regulated by o349 of the *wec* gene cluster of Escherichia coli K-12. *Journal of bacteriology* 181: 6564–8.

Bendezú, F. O., C. A. Hale, T. G. Bernhardt, and P. A. J. de Boer. 2009. RodZ (YfgA) is required for proper assembly of the MreB actin cytoskeleton and cell shape in *E. coli*. *The EMBO Journal* 28: 193–204. doi:10.1038/emboj.2008.264.

Bishop, R. E., H. S. Gibbons, T. Guina, M. S. Trent, S. I. Miller, and C. R. H. Raetz. 2000. Transfer of palmitate from phospholipids to lipid A in outer membranes of Gram-negative bacteria. *The EMBO Journal* 19: 5071–5080. doi:10.1093/emboj/19.19.5071.

Den Blaauwen, T., M. A. de Pedro, M. Nguyen-Distèche, and J. A. Ayala. 2008. Morphogenesis of rod-shaped sacculi. *FEMS Microbiology Reviews* 32. doi:10.1111/j.1574-6976.2007.00090.x.

Bligh, E. G., and W. J. Dyer. 1959. A rapid method of total lipid extraction and purification. *Canadian Journal of Biochemistry and Physiology* 37. NRC Research Press Ottawa, Canada: 911–917. doi:10.1139/o59-099.

Brooks, J. F., M. C. Gyllborg, D. C. Cronin, S. J. Quillin, C. A. Mallama, R. Foxall, C. Whistler, A. L. Goodman, et al. 2014. Global discovery of colonization determinants in the squid symbiont *Vibrio fischeri*. *Proceedings of the National Academy of Sciences of the United States of America* 111. National Academy of Sciences: 17284–9. doi:10.1073/pnas.1415957111.

Browning, D. F., T. J. Wells, F. L. S. França, F. C. Morris, Y. R. Sevastsyanovich, J. A. Bryant, M. D. Johnson, P. A. Lund, et al. 2013. Laboratory adapted *Escherichia coli*

K-12 becomes a pathogen of *Caenorhabditis elegans* upon restoration of O antigen biosynthesis. *Molecular Microbiology* 87. John Wiley & Sons, Ltd: 939–950. doi:10.1111/mmi.12144.

Buchan, D. W. A., and D. T. Jones. 2019. The PSIPRED Protein Analysis Workbench: 20 years on. *Nucleic Acids Research* 47. doi:10.1093/nar/gkz297.

Cain, A. K., L. Barquist, A. L. Goodman, I. T. Paulsen, J. Parkhill, and T. van Opijnen. 2020. A decade of advances in transposon-insertion sequencing. *Nature Reviews Genetics*. Nature Research. doi:10.1038/s41576-020-0244-x.

Cesar, S., and K. C. Huang. 2017. Thinking big: the tunability of bacterial cell size. *FEMS microbiology reviews*. Oxford University Press. doi:10.1093/femsre/fux026.

Chi, X., Q. Fan, Y. Zhang, K. Liang, L. Wan, Q. Zhou, and Y. Li. 2020. Structural mechanism of phospholipids translocation by MlaFEDB complex. *Cell Research* 30. Springer Nature: 1127–1135. doi:10.1038/s41422-020-00404-6.

Choi, J. S., W. Kim, S. Suk, H. Park, G. Bak, J. Yoon, and Y. Lee. 2018. The small RNA, SdsR, acts as a novel type of toxin in *Escherichia coli*. *RNA Biology* 15. Taylor and Francis Inc.: 1319–1335. doi:10.1080/15476286.2018.1532252.

Chong, Z. S., W. F. Woo, and S. S. Chng. 2015. Osmoporin OmpC forms a complex with MlaA to maintain outer membrane lipid asymmetry in *Escherichia coli*. *Molecular Microbiology* 98. Blackwell Publishing Ltd: 1133–1146. doi:10.1111/mmi.13202.

Clairfeuille, T., K. R. Buchholz, Q. Li, E. Verschueren, P. Liu, D. Sangaraju, S. Park, C. L. Noland, et al. 2020. Structure of the essential inner membrane lipopolysaccharide–PbgA complex. *Nature* 584. doi:10.1038/s41586-020-2597-x.

Danese, P. N., G. R. Oliver, K. Barr, G. D. Bowman, P. D. Rick, and T. J. Silhavy. 1998. Accumulation of the enterobacterial common antigen lipid II biosynthetic intermediate stimulates *degP* transcription in *Escherichia coli*. *Journal of bacteriology* 180: 5875–84.

Datsenko, K. A., and B. L. Wanner. 2000. One-step inactivation of chromosomal genes in *Escherichia coli* K-12 using PCR products. *Proceedings of the National Academy of Sciences of the United States of America* 97: 6640–5. doi:10.1073/pnas.120163297.

Deatherage, D. E., and J. E. Barrick. 2014. Identification of mutations in laboratory-evolved microbes from next-generation sequencing data using breseq. *Methods in molecular biology (Clifton, N.J.)* 1151. NIH Public Access: 165–88. doi:10.1007/978-1-4939-0554-6_12.

DeJesus, M. A., S. Nambi, C. M. Smith, R. E. Baker, C. M. Sassetti, and T. R. Ioerger. 2017. Statistical analysis of genetic interactions in Tn-Seq data. *Nucleic acids research* 45. Oxford University Press: e93. doi:10.1093/nar/gkx128.

Dixon, R. A., and I. Chopra. 1986. Leakage of periplasmic proteins from *Escherichia coli* mediated by polymyxin B nonapeptide. *Antimicrobial Agents and Chemotherapy* 29. American Society for Microbiology (ASM): 781–788. doi:10.1128/AAC.29.5.781.

Eddy, S. R. 2011. Accelerated profile HMM searches. *PLoS Computational Biology* 7. PLoS Comput Biol. doi:10.1371/journal.pcbi.1002195.

Ekiert, D. C., G. Bhabha, G. L. Isom, G. Greenan, S. Ovchinnikov, I. R. Henderson, J. S. Cox, and R. D. Vale. 2017. Architectures of Lipid Transport Systems for the Bacterial Outer Membrane. *Cell* 169: 273-285.e17. doi:10.1016/j.cell.2017.03.019.

Ercan, B., W. Y. Low, X. Liu, and S. S. Chng. 2019. Characterization of Interactions and Phospholipid Transfer between Substrate Binding Proteins of the OmpC-Mla System. *Biochemistry* 58. American Chemical Society: 114–119. doi:10.1021/acs.biochem.8b00897.

Fassel, T. A., P. E. Mozdziak, J. R. Sanger, and C. E. Edmiston. 1997. Paraformaldehyde effect on ruthenium red and lysine preservation and staining of

935 the staphylococcal glycocalyx. *Microscopy Research and Technique* 36. Microsc
936 Res Tech: 422–427. doi:10.1002/(SICI)1097-0029(19970301)36:5<422::AID-
937 JEMT12>3.0.CO;2-U.
938 Fivenson, E. M., and T. G. Bernhardt. 2020. An essential membrane protein modulates
939 the proteolysis of LpxC to control lipopolysaccharide synthesis in *Escherichia coli*.
940 *mBio* 11. American Society for Microbiology. doi:10.1128/mBio.00939-20.
941 Ganong, B. R., J. M. Leonard, and C. R. H. Raetz. 1980. Phosphatidic acid
942 accumulation in the membranes of *Escherichia coli* mutants defective in CDP-
943 diglyceride synthetase. *Journal of Biological Chemistry* 255. doi:10.1016/S0021-
944 9258(19)86078-7.
945 Garwin, J L, A. L. Klages, and J. E. Cronan. 1980. Beta-ketoacyl-acyl carrier protein
946 synthase II of *Escherichia coli*. Evidence for function in the thermal regulation of
947 fatty acid synthesis. *The Journal of biological chemistry* 255: 3263–5.
948 Garwin, J. L., A. L. Klages, and J. E. Cronan. 1980. *Structural, enzymatic, and genetic*
949 *studies of beta-ketoacyl-acyl carrier protein synthases I and II of* Escherichia coli.
950 *Journal of Biological Chemistry*. Vol. 255. doi:10.1016/S0021-9258(19)70226-9.
951 Glauner, B. 1988. Separation and quantification of muropeptides with high-performance
952 liquid chromatography. *Analytical Biochemistry* 172. Anal Biochem: 451–464.
953 doi:10.1016/0003-2697(88)90468-X.
954 Goehring, N. W., and J. Beckwith. 2005. Diverse paths to midcell: Assembly of the
955 bacterial cell division machinery. *Current Biology*. Cell Press.
956 doi:10.1016/j.cub.2005.06.038.
957 Goodall, E. C. A., A. Robinson, I. G. Johnston, S. Jabbari, K. A. Turner, A. F.
958 Cunningham, P. A. Lund, J. A. Cole, et al. 2018. The Essential Genome of
959 *Escherichia coli* K-12. Edited by Swaine L. Chen. *mBio* 9: e02096-17.
960 doi:10.1128/mBio.02096-17.
961 Guest, R. L., D. S. Guerra, M. Wissler, J. Grimm, and T. J. Silhavy. 2020. Yejm
962 modulates activity of the YciM/FtsH protease complex to prevent lethal
963 accumulation of lipopolysaccharide. *mBio* 11. American Society for Microbiology.
964 doi:10.1128/mBio.00598-20.
965 Harvey, P. C., M. Watson, S. Hulme, M. A. Jones, M. Lovell, A. Berchieri, J. Young, N.
966 Bumstead, et al. 2011. *Salmonella enterica* serovar typhimurium colonizing the
967 lumen of the chicken intestine grows slowly and upregulates a unique set of
968 virulence and metabolism genes. *Infection and immunity* 79. American Society for
969 Microbiology (ASM): 4105–21. doi:10.1128/IAI.01390-10.
970 Hill, N. S., P. J. Buske, Y. Shi, and P. A. Levin. 2013. A Moonlighting Enzyme Links
971 *Escherichia coli* Cell Size with Central Metabolism. Edited by Josep Casadesús.
972 *PLoS Genetics* 9. Public Library of Science: e1003663.
973 doi:10.1371/journal.pgen.1003663.
974 Hu, P., S. C. Janga, M. Babu, J. J. Díaz-Mejía, G. Butland, W. Yang, O. Pogoutse, X.
975 Guo, et al. 2009. Global functional atlas of *Escherichia coli* encompassing
976 previously uncharacterized proteins. *PLoS biology* 7: e96.
977 doi:10.1371/journal.pbio.1000096.
978 Hughes, G. W., S. C. L. Hall, C. S. Laxton, P. Sridhar, A. H. Mahadi, C. Hatton, T. J.
979 Piggot, P. J. Wotherspoon, et al. 2019. Evidence for phospholipid export from the
980 bacterial inner membrane by the Mla ABC transport system. *Nature Microbiology* 4.
981 Nature Publishing Group: 1692–1705. doi:10.1038/s41564-019-0481-y.
982 Isom, G. L., N. J. Davies, Z.-S. Chong, J. A. Bryant, M. Jamshad, M. Sharif, A. F.
983 Cunningham, T. J. Knowles, et al. 2017. MCE domain proteins: conserved inner
984 membrane lipid-binding proteins required for outer membrane homeostasis.
985 *Scientific Reports* 7: 8608. doi:10.1038/s41598-017-09111-6.
986 Jana, B., A. K. Cain, W. T. Doerrler, C. J. Boinett, M. C. Fookes, J. Parkhill, and L.

987 Guardabassi. 2017. The secondary resistome of multidrug-resistant *Klebsiella*
988 *pneumoniae*. *Scientific Reports* 7. Nature Publishing Group: 42483.
989 doi:10.1038/srep42483.
990 Jia, W., A. El Zoeiby, T. N. Petruzziello, B. Jayabalasingham, S. Seyedirashti, and R. E.
991 Bishop. 2004. Lipid trafficking controls endotoxin acylation in outer membranes of
992 *Escherichia coli*. *Journal of Biological Chemistry* 279. J Biol Chem: 44966–44975.
993 doi:10.1074/jbc.M404963200.
994 Jones, D. T. 1999. Protein secondary structure prediction based on position-specific
995 scoring matrices. *Journal of Molecular Biology* 292. Academic Press: 195–202.
996 doi:10.1006/jmbi.1999.3091.
997 Jorgenson, M. A., S. Kannan, M. E. Laubacher, and K. D. Young. 2016. Dead-end
998 intermediates in the enterobacterial common antigen pathway induce
999 morphological defects in *Escherichia coli* by competing for undecaprenyl
1000 phosphate. *Molecular Microbiology* 100: 1–14. doi:10.1111/mmi.13284.
1001 Jorgenson, M. A., W. J. MacCain, B. M. Meberg, S. Kannan, J. C. Bryant, and K. D.
1002 Young. 2019. Simultaneously inhibiting undecaprenyl phosphate production and
1003 peptidoglycan synthases promotes rapid lysis in *Escherichia coli*. *Molecular*
1004 *Microbiology* 112. Blackwell Publishing Ltd: 233–248. doi:10.1111/mmi.14265.
1005 Kalyaanamoorthy, S., B. Q. Minh, T. K. F. Wong, A. Von Haeseler, and L. S. Jermiin.
1006 2017. ModelFinder: Fast model selection for accurate phylogenetic estimates.
1007 *Nature Methods* 14. Nature Publishing Group: 587–589. doi:10.1038/nmeth.4285.
1008 Kanfer, J., and E. P. Kennedy. 1964. Metabolism and function of bacterial lipids. II.
1009 Biosynthesis of phospholipids in *Escherichia coli*. *The Journal of biological*
1010 *chemistry* 239. doi:10.1016/S0021-9258(18)91247-0.
1011 Kato, J. I., S. Fujisaki, K. I. Nakajima, Y. Nishimura, M. Sato, and A. Nakano. 1999. The
1012 *Escherichia coli* homologue of yeast Rer2, a key enzyme of dolichol synthesis, is
1013 essential for carrier lipid formation in bacterial cell wall synthesis. *Journal of*
1014 *Bacteriology* 181. American Society for Microbiology: 2733–2738.
1015 doi:10.1128/jb.181.9.2733-2738.1999.
1016 Katoh, K., and D. M. Standley. 2013. MAFFT multiple sequence alignment software
1017 version 7: Improvements in performance and usability. *Molecular Biology and*
1018 *Evolution* 30. Mol Biol Evol: 772–780. doi:10.1093/molbev/mst010.
1019 Kelley, L. A., S. Mezulis, C. M. Yates, M. N. Wass, and M. J. E. Sternberg. 2015. The
1020 Phyre2 web portal for protein modeling, prediction and analysis. *Nature protocols*
1021 10. Europe PMC Funders: 845–58. doi:10.1038/nprot.2015.053.
1022 Keseler, I. M., A. Mackie, A. Santos-Zavaleta, R. Billington, C. Bonavides-Martínez, R.
1023 Caspi, C. Fulcher, S. Gama-Castro, et al. 2017. The EcoCyc database: reflecting
1024 new knowledge about *Escherichia coli* K-12. *Nucleic Acids Research* 45. Oxford
1025 University Press: D543–D550. doi:10.1093/nar/gkw1003.
1026 Klein, G., N. Kobylak, B. Lindner, A. Stupak, and S. Raina. 2014. Assembly of
1027 lipopolysaccharide in *Escherichia coli* requires the essential LapB heat shock
1028 protein. *Journal of Biological Chemistry* 289. American Society for Biochemistry
1029 and Molecular Biology Inc.: 14829–14853. doi:10.1074/jbc.M113.539494.
1030 Knowles, T. J., A. Scott-Tucker, M. Overduin, and I. R. Henderson. 2009. Membrane
1031 protein architects: the role of the BAM complex in outer membrane protein
1032 assembly. *Nature Reviews Microbiology* 7: 206–214. doi:10.1038/nrmicro2069.
1033 Koboldt, D. C., Q. Zhang, D. E. Larson, D. Shen, M. D. McLellan, L. Lin, C. A. Miller, E.
1034 R. Mardis, et al. 2012. VarScan 2: Somatic mutation and copy number alteration
1035 discovery in cancer by exome sequencing. *Genome Research* 22: 568–576.
1036 doi:10.1101/gr.129684.111.
1037 Lai, G. C., H. Cho, and T. G. Bernhardt. 2017. The mecillinam resistome reveals a role
1038 for peptidoglycan endopeptidases in stimulating cell wall synthesis in *Escherichia*

1039 *coli*. *PLoS Genetics* 13. Public Library of Science.
1040 doi:10.1371/journal.pgen.1006934.
1041 Langmead, B., and S. L. Salzberg. 2012. Fast gapped-read alignment with Bowtie 2.
1042 *Nature methods* 9. NIH Public Access: 357–9. doi:10.1038/nmeth.1923.
1043 Langridge, G. C., M. D. Phan, D. J. Turner, T. T. Perkins, L. Parts, J. Haase, I. Charles,
1044 D. J. Maskell, et al. 2009. Simultaneous assay of every Salmonella Typhi gene
1045 using one million transposon mutants. *Genome Research* 19: 2308–2316.
1046 doi:10.1101/gr.097097.109.
1047 Li, G., K. Hamamoto, and M. Kitakawa. 2012. Inner Membrane Protein YhcB Interacts
1048 with RodZ Involved in Cell Shape Maintenance in *Escherichia coli*. *ISRN molecular*
1049 *biology* 2012: 304021. doi:10.5402/2012/304021.
1050 Li, H., B. Handsaker, A. Wysoker, T. Fennell, J. Ruan, N. Homer, G. Marth, G.
1051 Abecasis, et al. 2009. The Sequence Alignment/Map format and SAMtools.
1052 *Bioinformatics* 25: 2078–2079. doi:10.1093/bioinformatics/btp352.
1053 Li, Z., and T. Velkov. 2019. Polymyxins: Mode of Action. In *Advances in Experimental*
1054 *Medicine and Biology*, 1145:37–54. Springer New York LLC. doi:10.1007/978-3-
1055 030-16373-0_4.
1056 Liu, D., and P. R. Reeves. 1994. *Escherichia coli* K12 regains its O antigen.
1057 *Microbiology* 140: 49–57. doi:10.1099/13500872-140-1-49.
1058 Liu, X., Y. Yin, J. Wu, and Z. Liu. 2014. Structure and mechanism of an intramembrane
1059 liponucleotide synthetase central for phospholipid biosynthesis. *Nature*
1060 *Communications* 5. Nature Publishing Group: 1–10. doi:10.1038/ncomms5244.
1061 Lugtenberg, B. 1981. Composition and function of the outer membrane of *Escherichia*
1062 *coli*. *Trends in Biochemical Sciences*. Elsevier Current Trends. doi:10.1016/0968-
1063 0004(81)90095-5.
1064 Luirink, J., Z. Yu, S. Wagner, and J.-W. de Gier. 2012. Biogenesis of inner membrane
1065 proteins in *Escherichia coli*. *Biochimica et Biophysica Acta (BBA) - Bioenergetics*
1066 1817. Elsevier: 965–976. doi:10.1016/J.BBABIO.2011.12.006.
1067 Maddalo, G., F. Stenberg-Bruzell, H. Götzke, S. Toddo, P. Björkholm, H. Eriksson, P.
1068 Chovanec, P. Genevaux, et al. 2011. Systematic Analysis of Native Membrane
1069 Protein Complexes in *Escherichia coli*. *Journal of Proteome Research* 10: 1848–
1070 1859. doi:10.1021/pr101105c.
1071 Mahalakshmi, S., M. R. Sunayana, L. SaiSree, and M. Reddy. 2014. *yciM* is an
1072 essential gene required for regulation of lipopolysaccharide synthesis in
1073 *Escherichia coli*. *Molecular Microbiology* 91: 145–157. doi:10.1111/mmi.12452.
1074 Malinverni, J. C., and T. J. Silhavy. 2009. An ABC transport system that maintains lipid
1075 asymmetry in the Gram-negative outer membrane. *Proceedings of the National*
1076 *Academy of Sciences* 106: 8009–8014. doi:10.1073/pnas.0903229106.
1077 Martorana, A. M., S. Motta, D. Di Silvestre, F. Falchi, G. Dehò, P. Mauri, P. Sperandeo,
1078 and A. Polissi. 2014. Dissecting *Escherichia coli* Outer Membrane Biogenesis
1079 Using Differential Proteomics. Edited by Riccardo Manganelli. *PLoS ONE* 9. Public
1080 Library of Science: e100941. doi:10.1371/journal.pone.0100941.
1081 Matsumoto, K., M. Okada, Y. Horikoshi, H. Matsuzaki, T. Kishi, M. Itaya, and I. Shibuya.
1082 1998. Cloning, sequencing, and disruption of the *Bacillus subtilis psd* gene coding
1083 for phosphatidylserine decarboxylase. *Journal of Bacteriology* 180. American
1084 Society for Microbiology: 100–106. doi:10.1128/jb.180.1.100-106.1998.
1085 Matsuyama, S., T. Tajima, and H. Tokuda. 1995. A novel periplasmic carrier protein
1086 involved in the sorting and transport of Escherichia coli lipoproteins destined for the
1087 outer membrane. *The EMBO journal* 14: 3365–72.
1088 Matsuyama, S. I., N. Yokota, and H. Tokuda. 1997. A novel outer membrane
1089 lipoprotein, LolB (HemM), involved in the LolA (p20)-dependent localization of
1090 lipoproteins to the outer membrane of Escherichia coli. *EMBO Journal* 16. Wiley-

1091 VCH Verlag: 6947–6955. doi:10.1093/emboj/16.23.6947.
1092 May, J. M., D. J. Sherman, B. W. Simpson, N. Ruiz, and D. Kahne. 2015.
1093 Lipopolysaccharide transport to the cell surface: Periplasmic transport and
1094 assembly into the outer membrane. *Philosophical Transactions of the Royal*
1095 *Society B: Biological Sciences*. Royal Society of London.
1096 doi:10.1098/rstb.2015.0027.
1097 May, K. L., and T. J. Silhavy. 2018. The *Escherichia coli* Phospholipase PldA Regulates
1098 Outer Membrane Homeostasis via Lipid Signaling. Edited by Susan Gottesman.
1099 *mBio* 9. doi:10.1128/mBio.00379-18.
1100 Mehla, J., G. Liechti, R. M. Morgenstein, J. H. Caufield, A. Hosseinnia, A. Gagarinova,
1101 S. Phanse, M. Brockett, et al. 2021. YhcB (DUF1043), a novel cell division protein
1102 conserved across gamma-proteobacteria 1. *bioRxiv*. Cold Spring Harbor
1103 Laboratory: 2020.12.31.425005. doi:10.1101/2020.12.31.425005.
1104 Mengin-Lecreulx, D., C. Michaud, C. Richaud, D. Blanot, and J. van Heijenoort. 1988.
1105 Incorporation of LL-diaminopimelic acid into peptidoglycan of *Escherichia coli*
1106 mutants lacking diaminopimelate epimerase encoded by *dapF*. *Journal of*
1107 *bacteriology* 170: 2031–9.
1108 Mi, H., D. Ebert, A. Muruganujan, C. Mills, L. P. Albou, T. Mushayamaha, and P. D.
1109 Thomas. 2021. PANTHER version 16: a revised family classification, tree-based
1110 classification tool, enhancer regions and extensive API. *Nucleic acids research* 49.
1111 NLM (Medline): D394–D403. doi:10.1093/nar/gkaa1106.
1112 Mogi, T., E. Mizuochi-Asai, S. Endou, S. Akimoto, and H. Nakamura. 2006. Role of a
1113 putative third subunit YhcB on the assembly and function of cytochrome bd-type
1114 ubiquinol oxidase from *Escherichia coli*. *Biochimica et Biophysica Acta (BBA) -*
1115 *Bioenergetics* 1757: 860–864. doi:10.1016/j.bbabio.2006.05.043.
1116 Molloy, M. P., B. R. Herbert, M. B. Slade, T. Rabilloud, A. S. Nouwens, K. L. Williams,
1117 and A. A. Gooley. 2000. Proteomic analysis of the *Escherichia coli* outer
1118 membrane. *European Journal of Biochemistry* 267. John Wiley & Sons, Ltd: 2871–
1119 2881. doi:10.1046/j.1432-1327.2000.01296.x.
1120 Nelson, D. E., and K. D. Young. 2000. Penicillin binding protein 5 affects cell diameter,
1121 contour, and morphology of Escherichia coli. *Journal of Bacteriology* 182. American
1122 Society for Microbiology Journals: 1714–1721. doi:10.1128/JB.182.6.1714-
1123 1721.2000.
1124 Nelson, D. E., and K. D. Young. 2001. Contributions of PBP 5 and DD-
1125 carboxypeptidase penicillin binding proteins to maintenance of cell shape in
1126 *Escherichia coli*. *Journal of Bacteriology* 183. American Society for Microbiology
1127 Journals: 3055–3064. doi:10.1128/JB.183.10.3055-3064.2001.
1128 Newton, B. A. 1953. Reversal of the antibacterial activity of polymyxin by divalent
1129 cations [2]. *Nature*. Nature Publishing Group. doi:10.1038/172160a0.
1130 Nguyen, L. T., H. A. Schmidt, A. Von Haeseler, and B. Q. Minh. 2015. IQ-TREE: A fast
1131 and effective stochastic algorithm for estimating maximum-likelihood phylogenies.
1132 *Molecular Biology and Evolution* 32. Oxford University Press: 268–274.
1133 doi:10.1093/molbev/msu300.
1134 Nichols, R. J., S. Sen, Y. J. Choo, P. Beltrao, M. Zietek, R. Chaba, S. Lee, K. M.
1135 Kazmierczak, et al. 2011. Phenotypic landscape of a bacterial cell. *Cell* 144: 143–
1136 56. doi:10.1016/j.cell.2010.11.052.
1137 Nikaido, H. 2005. Restoring permeability barrier function to outer membrane. *Chemistry*
1138 *& biology* 12. Elsevier: 507–9. doi:10.1016/j.chembiol.2005.05.001.
1139 Nikaido, H., and M. Vaara. 1985. Molecular basis of bacterial outer membrane
1140 permeability. *Microbiology and Molecular Biology Reviews* 49.
1141 Ogura, T., K. Inoue, T. Tatsuta, T. Suzaki, K. Karata, K. Young, L. H. Su, C. A. Fierke,
1142 et al. 1999. Balanced biosynthesis of major membrane components through

1143 regulated degradation of the committed enzyme of lipid A biosynthesis by the AAA
1144 protease FtsH (HflB) in *Escherichia coli*. *Molecular microbiology* 31: 833–44.
1145 Okuda, S., and H. Tokuda. 2011. Lipoprotein sorting in bacteria. *Annual Review of*
1146 *Microbiology* 65. Annu Rev Microbiol: 239–259. doi:10.1146/annurev-micro-
1147 090110-102859.
1148 Okuda, S., D. J. Sherman, T. J. Silhavy, N. Ruiz, and D. Kahne. 2016.
1149 Lipopolysaccharide transport and assembly at the outer membrane: The PEZ
1150 model. *Nature Reviews Microbiology*. Nature Publishing Group.
1151 doi:10.1038/nrmicro.2016.25.
1152 Page, A. J., S. Bastkowski, M. Yasir, A. K. Turner, T. Le Viet, G. M. Savva, M. A.
1153 Webber, and I. G. Charles. 2020. AlbaTraDIS: Comparative analysis of large
1154 datasets from parallel transposon mutagenesis experiments. Edited by Mihaela
1155 Pertea. *PLOS Computational Biology* 16. Public Library of Science: e1007980.
1156 doi:10.1371/journal.pcbi.1007980.
1157 Pearson, W. R., T. Wood, Z. Zhang, and W. Miller. 1997. Comparison of DNA
1158 Sequences with Protein Sequences. *Genomics* 46: 24–36.
1159 doi:10.1006/geno.1997.4995.
1160 Pierucci, O. 1978. Dimensions of *Escherichia coli* at various growth rates: model for
1161 envelope growth. *Journal of Bacteriology* 135. J Bacteriol: 559–574.
1162 doi:10.1128/jb.135.2.559-574.1978.
1163 Polissi, A., and P. Sperandeo. 2014. The lipopolysaccharide export pathway in
1164 *Escherichia coli*: structure, organization and regulated assembly of the Lpt
1165 machinery. *Marine drugs* 12. Multidisciplinary Digital Publishing Institute (MDPI):
1166 1023–42. doi:10.3390/md12021023.
1167 Powers, M. J., and M. S. Trent. 2018. Phospholipid retention in the absence of
1168 asymmetry strengthens the outer membrane permeability barrier to last-resort
1169 antibiotics. *Proceedings of the National Academy of Sciences of the United States*
1170 *of America* 115. National Academy of Sciences: E8518–E8527.
1171 doi:10.1073/pnas.1806714115.
1172 Ramos-Morales, F., A. I. Prieto, C. R. Beuzón, D. W. Holden, and J. Casadesús. 2003.
1173 Role for *Salmonella enterica* enterobacterial common antigen in bile resistance and
1174 virulence. *Journal of bacteriology* 185: 5328–32.
1175 Richaud, C., W. Higgins, D. Mengin-Lecreulx, and P. Stragier. 1987. Molecular cloning,
1176 characterization, and chromosomal localization of *dapF*, the *Escherichia coli* gene
1177 for diaminopimelate epimerase. *Journal of bacteriology* 169: 1454–9.
1178 Robinson, M. D., D. J. McCarthy, and G. K. Smyth. 2009. edgeR: A Bioconductor
1179 package for differential expression analysis of digital gene expression data.
1180 *Bioinformatics* 26. Oxford University Press: 139–140.
1181 doi:10.1093/bioinformatics/btp616.
1182 Rowlett, V. W., V. K. P. S. Mallampalli, A. Karlstaedt, W. Dowhan, H. Taegtmeyer, W.
1183 Margolin, and H. Vitrac. 2017. Impact of Membrane Phospholipid Alterations in
1184 *Escherichia coli* on Cellular Function and Bacterial Stress Adaptation. *Journal of*
1185 *bacteriology* 199. American Society for Microbiology Journals: e00849-16.
1186 doi:10.1128/JB.00849-16.
1187 Ruiz, N., B. Falcone, D. Kahne, and T. J. Silhavy. 2005. Chemical Conditionality: A
1188 GeneticStrategy to Probe Organelle Assembly. *Cell* 121. Cell Press: 307–317.
1189 doi:10.1016/J.CELL.2005.02.014.
1190 Saha, C. K., R. Sanches Pires, H. Brolin, M. Delannoy, and G. C. Atkinson. 2020. FlaGs
1191 and webFlaGs: discovering novel biology through the analysis of gene
1192 neighbourhood conservation. Edited by Alfonso Valencia. *Bioinformatics*. Oxford
1193 University Press (OUP). doi:10.1093/bioinformatics/btaa788.
1194 Schaechter, M., O. MaalOe, and N. O. Kjeldgaard. 1958. Dependency on Medium and

Temperature of Cell Size and Chemical Composition during Balanced Growth of *Salmonella* typhimurium. *Journal of General Microbiology* 19. Microbiology Society: 592–606. doi:10.1099/00221287-19-3-592.

Schindelin, J., I. Arganda-Carreras, E. Frise, V. Kaynig, M. Longair, T. Pietzsch, S. Preibisch, C. Rueden, et al. 2012. Fiji: An open-source platform for biological-image analysis. *Nature Methods*. doi:10.1038/nmeth.2019.

Sherman, D. J., R. Xie, R. J. Taylor, A. H. George, S. Okuda, P. J. Foster, D. J. Needleman, and D. Kahne. 2018. Lipopolysaccharide is transported to the cell surface by a membrane-to-membrane protein bridge. *Science*. doi:10.1126/SCIENCE.AAR1886.

Shiomi, D., M. Sakai, and H. Niki. 2008. Determination of bacterial rod shape by a novel cytoskeletal membrane protein. *The EMBO journal* 27. European Molecular Biology Organization: 3081–91. doi:10.1038/emboj.2008.234.

Shrivastava, R., and S. S. Chng. 2019. Lipid trafficking across the Gram-negative cell envelope. *Journal of Biological Chemistry* 294. American Society for Biochemistry and Molecular Biology Inc.: 14175–14184. doi:10.1074/jbc.AW119.008139.

Silhavy, T. J., D. Kahne, and S. Walker. 2010. The bacterial cell envelope. *Cold Spring Harbor perspectives in biology* 2: a000414. doi:10.1101/cshperspect.a000414.

Simpson, B. W., J. M. May, D. J. Sherman, D. Kahne, and N. Ruiz. 2015. Lipopolysaccharide transport to the cell surface: biosynthesis and extraction from the inner membrane. *Philosophical transactions of the Royal Society of London. Series B, Biological sciences* 370. The Royal Society. doi:10.1098/rstb.2015.0029.

Singh, S. K., L. SaiSree, R. N. Amrutha, and M. Reddy. 2012. Three redundant murein endopeptidases catalyse an essential cleavage step in peptidoglycan synthesis of *Escherichia coli* K12. *Molecular Microbiology* 86: 1036–1051. doi:10.1111/mmi.12058.

Singh, S. K., S. Parveen, L. SaiSree, and M. Reddy. 2015. Regulated proteolysis of a cross-link-specific peptidoglycan hydrolase contributes to bacterial morphogenesis. *Proceedings of the National Academy of Sciences of the United States of America* 112. National Academy of Sciences: 10956–61. doi:10.1073/pnas.1507760112.

Sperandeo, P., F. K. Lau, A. Carpentieri, C. De Castro, A. Molinaro, G. Dehò, T. J. Silhavy, and A. Polissi. 2008. Functional analysis of the protein machinery required for transport of lipopolysaccharide to the outer membrane of *Escherichia coli*. *Journal of Bacteriology* 190. J Bacteriol: 4460–4469. doi:10.1128/JB.00270-08.

Spratt, B. G., and J. L. Strominger. 1976. Identification of the major penicillin binding proteins of *Escherichia coli* as D alanine carboxypeptidase IA. *Journal of Bacteriology* 127. American Society for Microbiology (ASM): 660–663. doi:10.1128/jb.127.1.660-663.1976.

Sullivan, N. F., and W. D. Donachie. 1984. Transcriptional organization within an *Escherichia coli* cell division gene cluster: Direction of transcription of the cell separation gene envA. *Journal of Bacteriology* 160: 724–732. doi:10.1128/jb.160.2.724-732.1984.

Sung, C. G., U. Choi, and C. R. Lee. 2020. Phenotypic characterization of a conserved inner membrane protein YhcB in Escherichia coli. *Journal of Microbiology* 58. Microbiological Society of Korea: 598–605. doi:10.1007/s12275-020-0078-4.

Tadokoro, A., H. Hayashi, T. Kishimoto, Y. Makino, S. Fujisaki, and Y. Nishimura. 2004. Interaction of the *Escherichia coli* Lipoprotein NlpI with Periplasmic Prc (Tsp) Protease. *Journal of Biochemistry* 135. J Biochem: 185–191. doi:10.1093/jb/mvh022.

Templin, M. F., A. Ursinus, and J. V. Höltje. 1999. A defect in cell wall recycling triggers autolysis during the stationary growth phase of *Escherichia coli*. *EMBO Journal* 18. EMBO J: 4108–4117. doi:10.1093/emboj/18.15.4108.

Thomason, L. C., N. Costantino, and D. L. Court. 2007. *E. coli* Genome Manipulation by P1 Transduction. In *Current Protocols in Molecular Biology*, Chapter 1:1.17.1-1.17.8. Hoboken, NJ, USA: John Wiley & Sons, Inc. doi:10.1002/0471142727.mb0117s79.

Thong, S., B. Ercan, F. Torta, Z. Y. Fong, H. Y. A. Wong, M. R. Wenk, and S.-S. Chng. 2016. Defining key roles for auxiliary proteins in an ABC transporter that maintains bacterial outer membrane lipid asymmetry. *eLife* 5. eLife Sciences Publications, Ltd. doi:10.7554/eLife.19042.

Trimble, M. J., P. Mlynárčik, M. Kolář, and R. E. W. Hancock. 2016. Polymyxin: Alternative mechanisms of action and resistance. *Cold Spring Harbor Perspectives in Medicine* 6. Cold Spring Harbor Laboratory Press: a025288. doi:10.1101/cshperspect.a025288.

Turner, A. K., M. Yasir, S. Bastkowski, A. Telatin, A. J. Page, I. G. Charles, and M. A. Webber. 2020. A genome-wide analysis of Escherichia coli responses to fosfomycin using TraDIS-Xpress reveals novel roles for phosphonate degradation and phosphate transport systems. *Journal of Antimicrobial Chemotherapy* 75. Oxford University Press: 3144–3151. doi:10.1093/jac/dkaa296.

Vadia, S., and P. A. Levin. 2015. Growth rate and cell size: A re-examination of the growth law. *Current Opinion in Microbiology*. Elsevier Ltd. doi:10.1016/j.mib.2015.01.011.

Vadia, S., J. L. Tse, R. Lucena, Z. Yang, D. R. Kellogg, J. D. Wang, and P. A. Levin. 2017. Fatty Acid Availability Sets Cell Envelope Capacity and Dictates Microbial Cell Size. *Current Biology* 27: 1757-1767.e5. doi:10.1016/j.cub.2017.05.076.

Walser, P. J., N. Ariotti, M. Howes, C. Ferguson, R. Webb, D. Schwudke, N. Leneva, K.-J. Cho, et al. 2012. Constitutive Formation of Caveolae in a Bacterium. *Cell* 150: 752–763. doi:10.1016/j.cell.2012.06.042.

Wu, T., J. Malinverni, N. Ruiz, S. Kim, T. J. Silhavy, and D. Kahne. 2005. Identification of a multicomponent complex required for outer membrane biogenesis in *Escherichia coli*. *Cell* 121. Elsevier B.V.: 235–245. doi:10.1016/j.cell.2005.02.015.

Yakushi, T., K. Masuda, S. I. Narita, S. I. Matsuyama, and H. Tokuda. 2000. A new ABC transporter mediating the detachment of lipid-modified proteins from membranes. *Nature Cell Biology* 2. Nat Cell Biol: 212–218. doi:10.1038/35008635.

Yethon, J. A., J. S. Gunn, R. K. Ernst, S. I. Miller, L. Laroche, D. Malo, and C. Whitfield. 2000. *Salmonella enterica* serovar Typhimurium waaP mutants show increased susceptibility to polymyxin and loss of virulence in vivo. *Infection and Immunity* 68. American Society for Microbiology (ASM): 4485–4491. doi:10.1128/IAI.68.8.4485-4491.2000.

Zheng, L., Y. Lin, S. Lu, J. Zhang, and M. Bogdanov. 2017. Biogenesis, transport and remodeling of lysophospholipids in Gram-negative bacteria. *Biochimica et Biophysica Acta - Molecular and Cell Biology of Lipids*. Elsevier B.V. doi:10.1016/j.bbalip.2016.11.015.

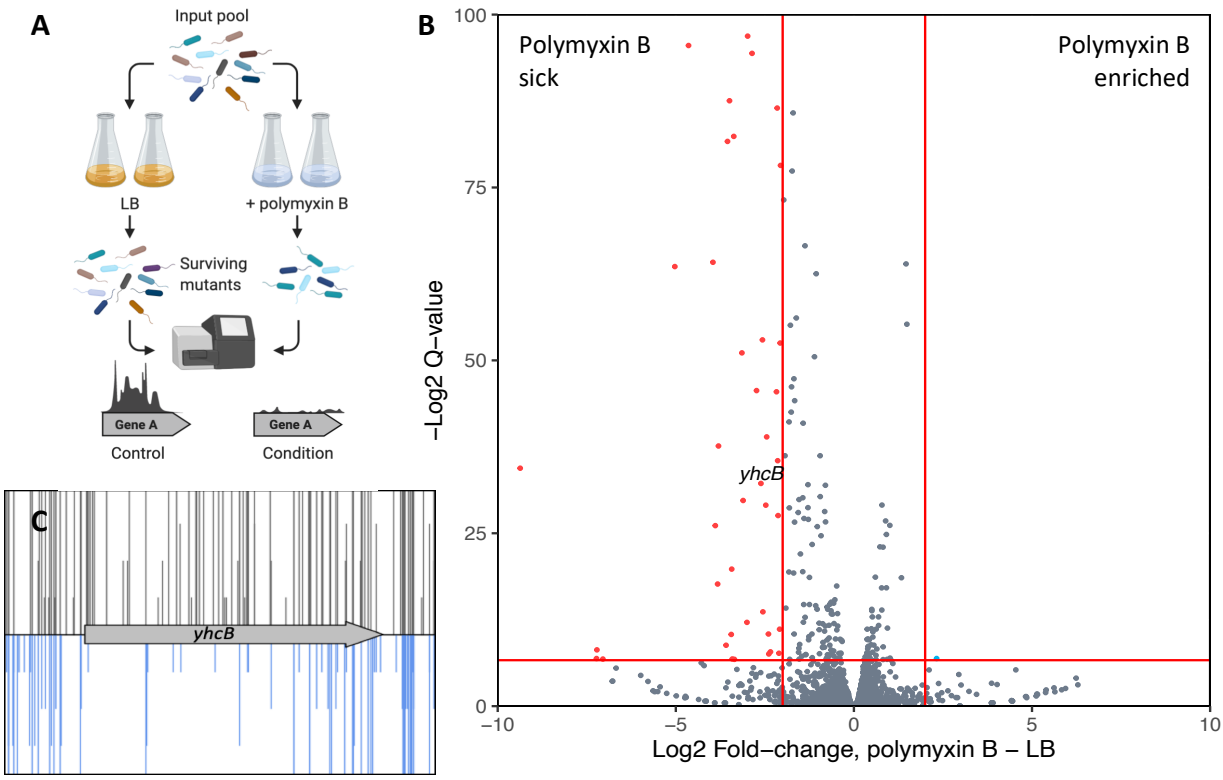

Figure 1. Screening the BW25113 transposon library in sub-inhibitory concentrations of polymyxin B

(A) Schematic showing the TIS experiment for identification of polymyxin B-sensitive mutants. (B) Volcano plot of the fold-change in mapped reads between conditions, calculated using BioTraDIS. Datapoints in red correspond with genes with >2-fold decrease in reads in the polymyxin B dataset relative to the LB outgrowth dataset, and with a Q-value > 0.01 (red horizontal line). While one datapoint in blue had a >2-fold increase in reads in polymyxin B dataset relative to the control, and a Q-value > 0.01. A label for the *yhcB* datapoint has been added above the point for clarity. (C) Image of the *yhcB* insertion data following outgrowth in LB only (grey, above) or in LB supplemented with polymyxin B (blue, below). The transposon insertion position along the gene is marked by a vertical line, with the vertical line size corresponding with read depth, with visibly fewer transposon-insertion sites identified within *yhcB* following outgrowth in LB supplemented with polymyxin B.

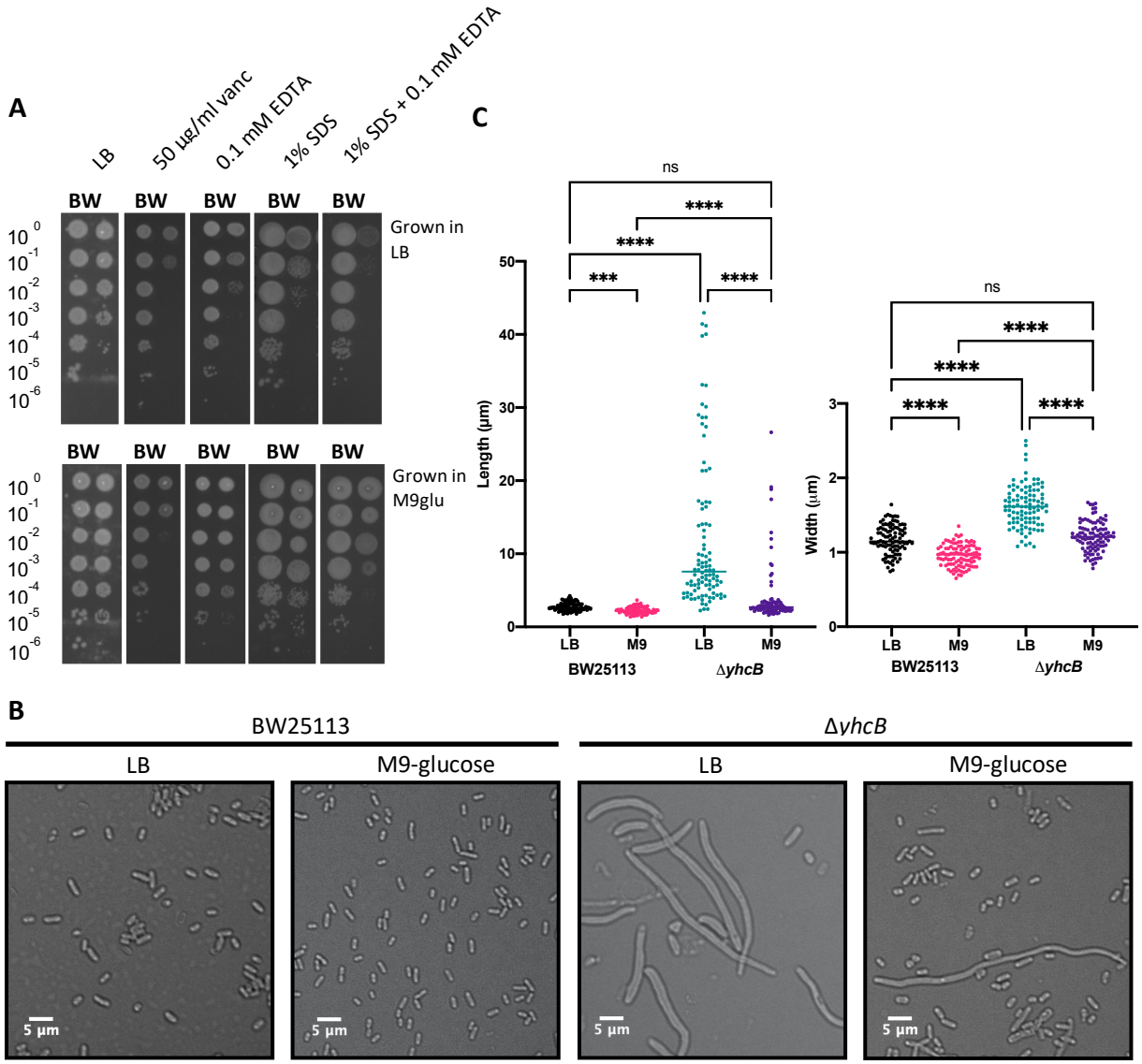

Figure 2. Validation of a *yhcB* mutant cell envelope defect and the effect of growth medium on cell size

(A) Overnight cultures of the WT strain BW25113 (BW) and Δ*yhcB* (Y) strain grown in LB or M9-glucose at 37˚C, normalised to an OD_{600} of 1.00 and 10-fold serially diluted before inoculating LB agar plates supplemented with various compounds. (B) The WT and Δ*yhcB* mutant were grown overnight in LB or M9-glucose media at 37˚C. Cells were visualised using a Nikon 90i microscope, a 5 µm bar is shown for scale. (C) Cell measurements for BW25113 and Δ*yhcB* mutant grown in LB and M9-glucose. Images were taken after overnight growth and are representative of n=4 experiments, data from 1 experiment is presented. Width and Length measurements were taken of 100 cells in each condition. A Kruskal-Wallis test with Dunn's correction for multiple comparisons was used to compare between samples: $p < 0.0001$ (****); $p < 0.0002$ (***).

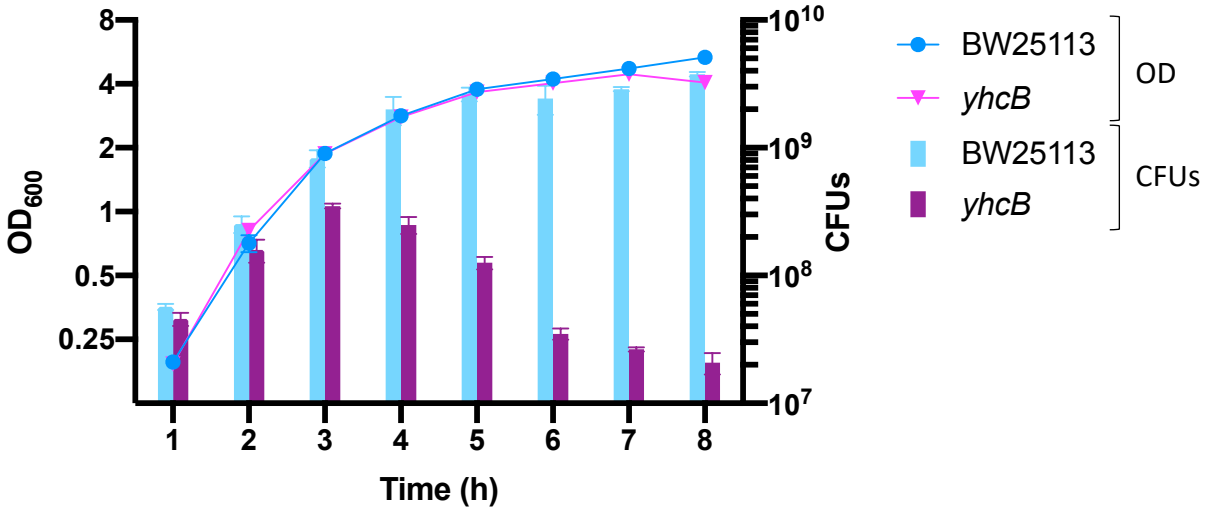

1319

1320 **Figure 3. The effect of *yhcB*–deletion during growth in rich media**

1321 (A) The optical density (OD) and number of colony forming units (CFUs) were recorded
1322 hourly over 8 h during growth in LB at 37˚C. Strains were grown in triplicate, the mean is
1323 plotted and the s.d. represented by error bars. BW25113 is shown in blue (•), *yhcB* is
1324 shown in pink (▾).

1325

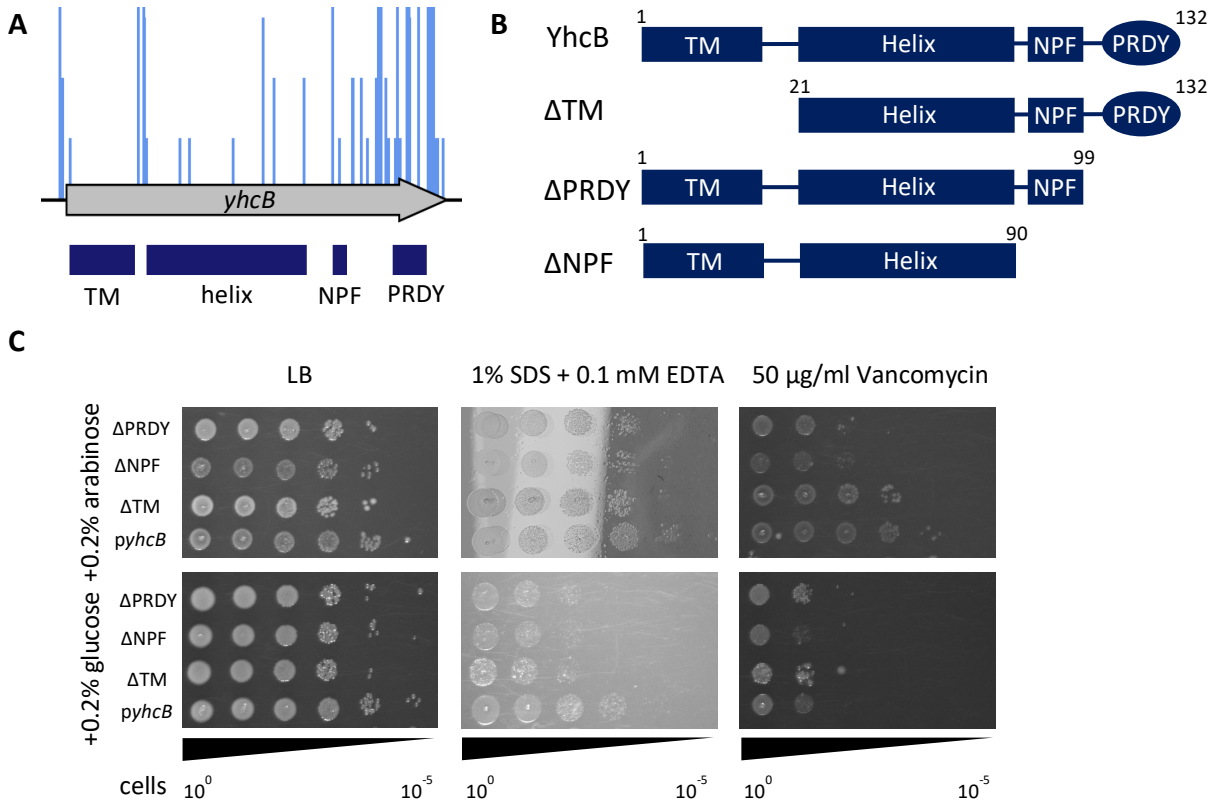

Figure 4. The structural and functional contribution of the domains of YhcB
(A) Polymyxin B TIS screen data (blue insertions) with the domains of YhcB mapped underneath (dark blue boxes). (B) Schematics of the plasmid-based YhcB complementation constructs. (C) Overnight cultures grown in LB supplemented with carbenicillin (for plasmid selection), normalised to an OD_{600} of 1.00 and 10-fold serially diluted before inoculating LB agar plates supplemented with vancomycin or SDS and EDTA, with 0.2% arabinose or 0.2% glucose.

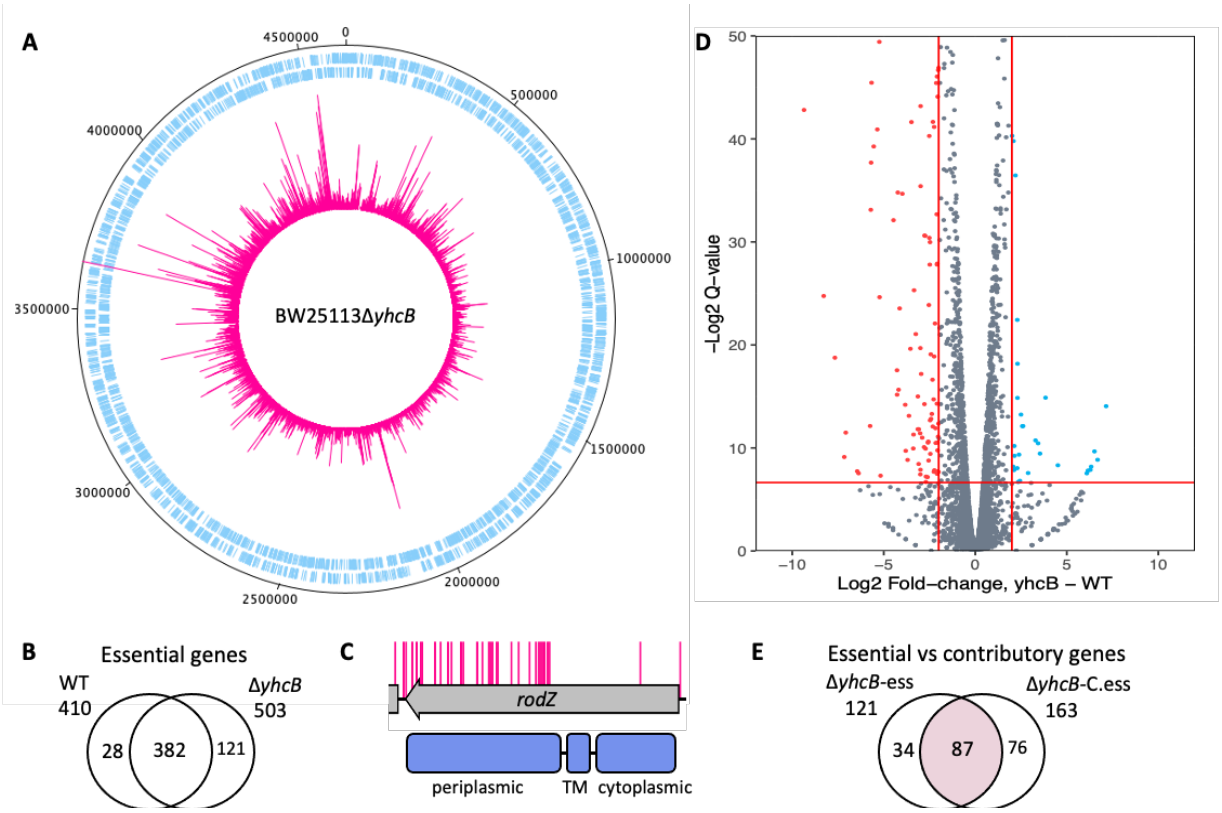

Figure 5. Construction of a transposon library in a *yhcB* mutant and identification of genes with a synthetic lethal relationship with *yhcB*

(A) The Δ*yhcB* transposon library. A genome map of BW25113 starting at the annotation origin with the sense and antisense coding sequences of BW25113 shown in blue, respectively, and the position and frequency of sequenced transposon insertion events shown in pink. (B) Comparison of genes identified by bimodal analysis as significantly underrepresented by transposon mutants in each library. (C) The insertion profile of *rodZ* in the Δ*yhcB* library, with RodZ domains shown below in blue. (D) The $\log_2$ fold-change of read depth per gene between the parent BW25113 and the Δ*yhcB* transposon library. Genes enriched for transposon insertions (>2-fold) in the *yhcB* library are shown in blue, indicative of more fit mutants. Genes with a >2-fold decrease in insertions are shown in red, indicative of sick mutants. A Q-value threshold of 0.01 was used (red horizontal line) (E) Comparison of genes predicted to be essential (sparsely disrupted genes) with genes identified as having a >2-fold decrease in reads compared to the control library (genes that contribute to fitness). This is a comparison of the bi-modal and enrichment analyses outputs. The overlap of these analyses are the 87 identified synthetic lethal genes (pink).

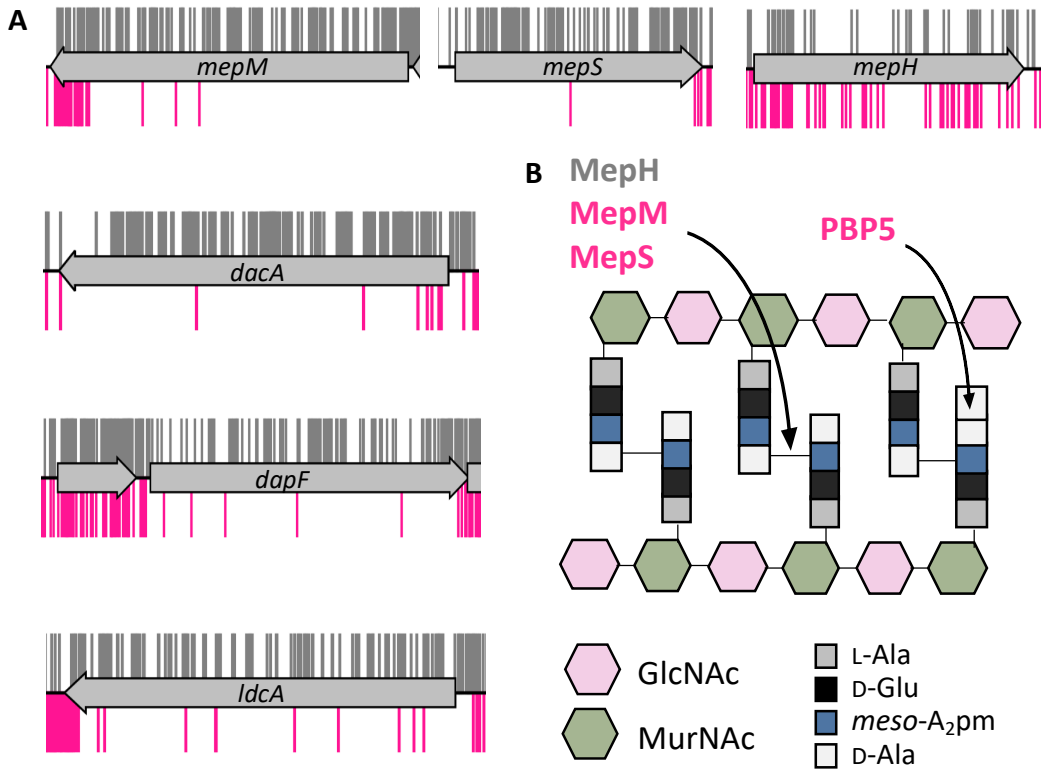

Figure 6. *yhcB* is synthetically lethal with components of PG synthesis and recycling pathways

(A) TIS data of the BW25113 library (grey) and BW25113Δ*yhcB* library (pink) were plotted above and below the gene track, respectively. Insertion sites are represented by vertical bars and are capped at a frequency of 1. (B) Schematic representation of the target sites of the endopeptidases and PBP5 (encoded by *dacA*). Abbreviations: *meso*-diaminopimelate (*meso*-A_2pm); N-acetylglucosamine (GlcNAc); N-acetylmuramic acid (MurNAc); L-Ala, L-alanine; D-Glu, D-glutamic acid; D-Ala, D-alanine.

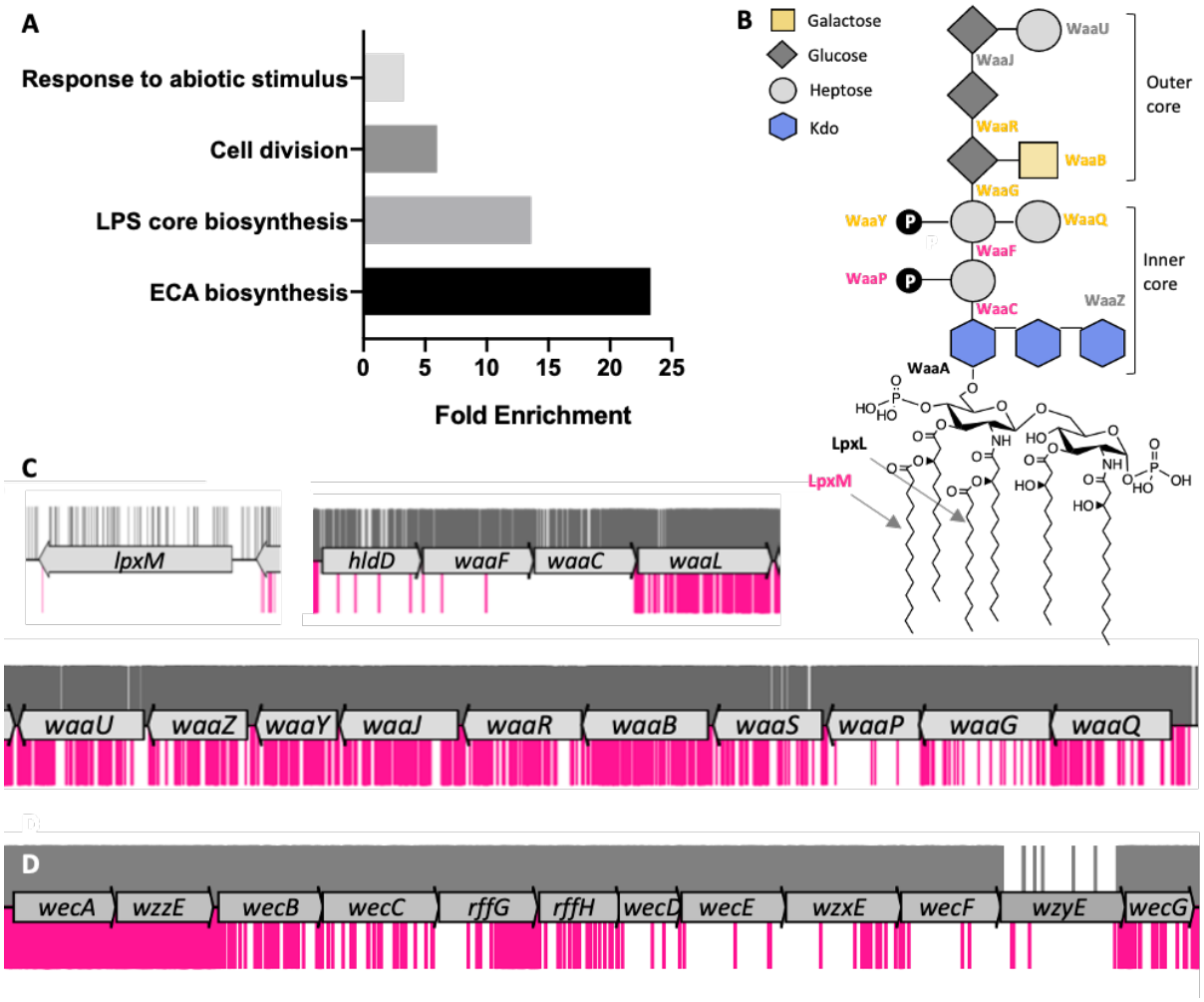

Figure 7. Functional enrichment among synthetic lethal genes
(A) Functional enrichment of cellular processes among the genes that are synthetically lethal with *yhcB*. Fisher's exact test with Bonferroni correction for multiple testing. Results displayed for $P < 0.05$. (B) A schematic of the structure of LPS. LPS biosynthesis enzymes are indicated next to the linkage they form (central column) or component they ligate (side branches). Synthetic lethal enzymes are labelled in dark pink, enzymes that contribute to fitness are labelled in orange, core essential enzymes in black and non-essential enzymes in grey. (C) TIS data for BW25113 (grey) and BW25113Δ*yhcB* (pink) libraries were plotted above and below the gene track, respectively. Insertion sites are represented by vertical bars and are capped at a frequency of 1. Insertions within genes required for LPS core biosynthesis, and *lpxM*, are significantly underrepresented. (D) The insertion profiles in genes of the enterobacterial common antigen biosynthetic pathway. Abbreviations: Lipopolysaccharide (LPS); Enterobacterial Common Antigen (ECA).

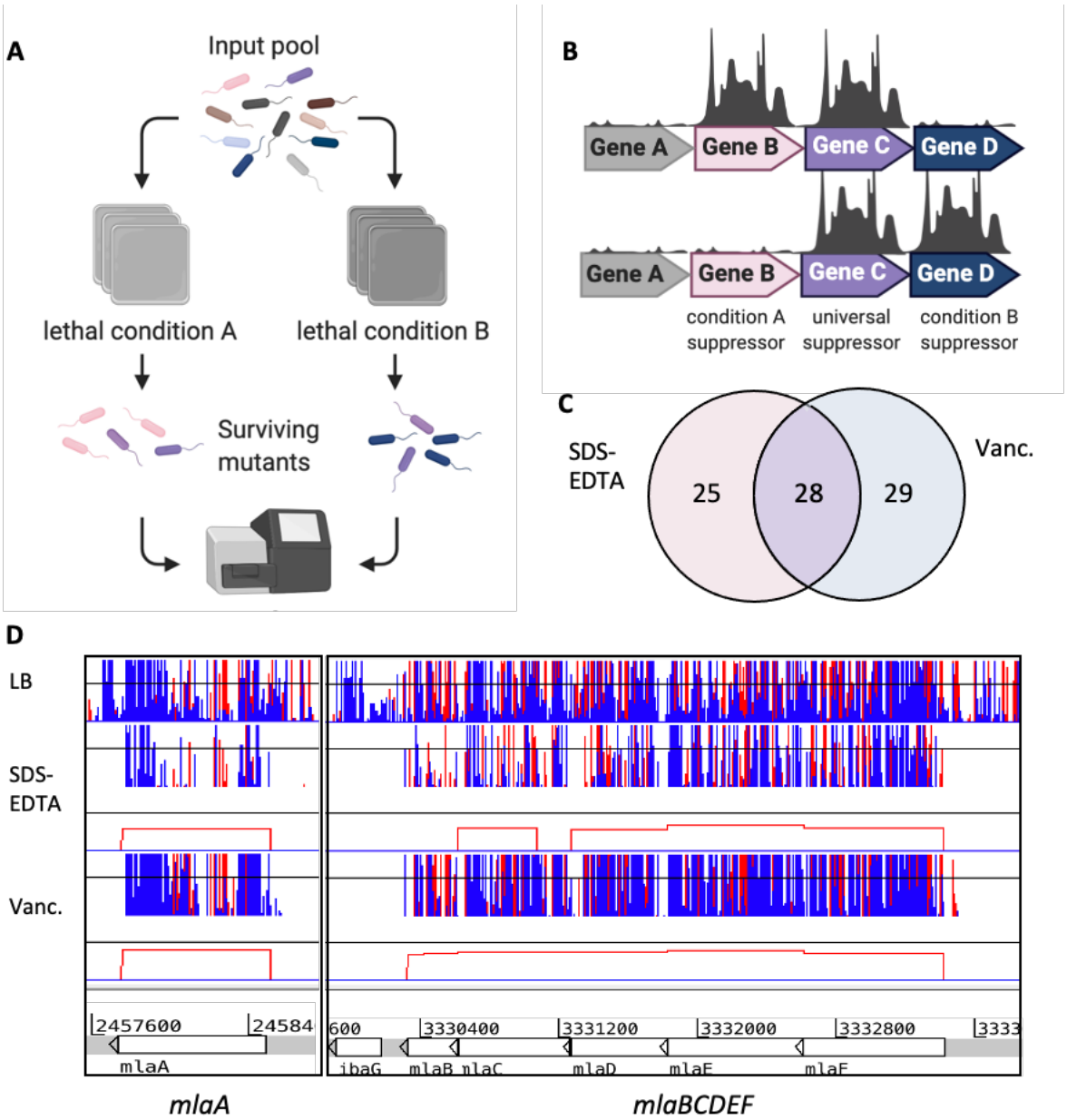

Figure 8. Identification of suppressor mutations that restore a *yhcB*-deletion defect (A) Experimental overview. (B) Cartoon of output. (C) Overlap between gene-deletion suppressors identified in the lower concentration vancomycin and SDS + EDTA screens. (D) Transposon insertion data for suppressor screens. Red and blue lines indicate the transposon insertion position corresponding with the transposon orientation at the point of insertion. The height of the bar corresponds with mapped sequencing read frequency. The red boxes underneath each suppressor dataset represent significant differential abundance of insertions of the condition compared to the control, identified by AlbaTraDIS. Panel A and B schematics created with BioRender.com, Panel D insertion plots visualised in Artemis (Rutherford et al. 2000).

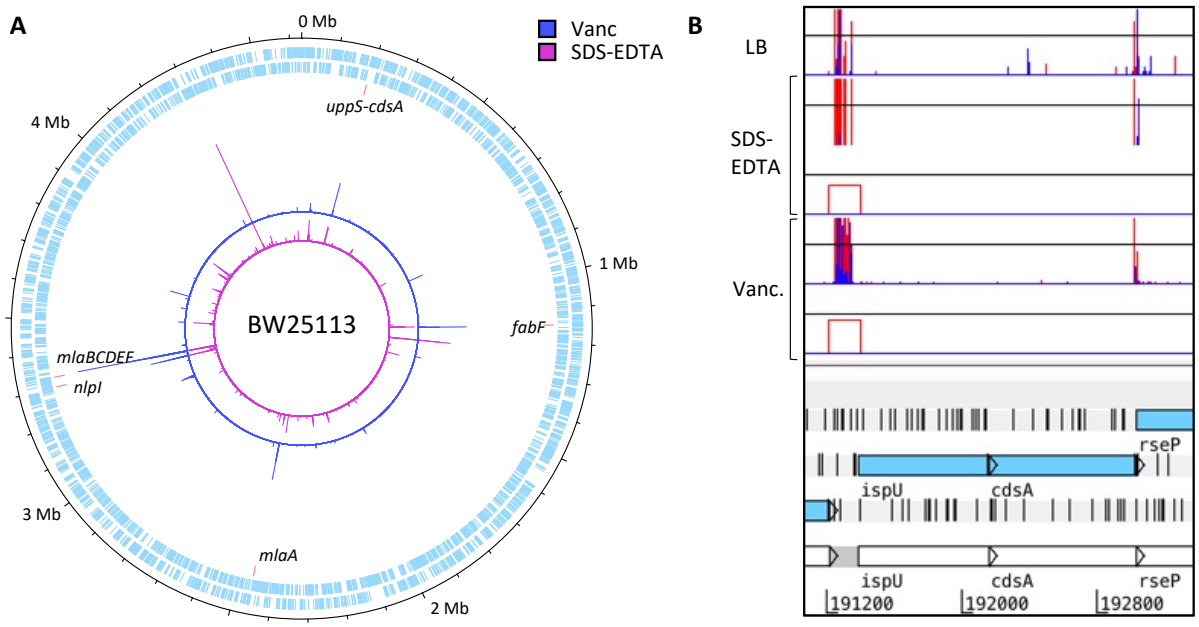

Figure 9. The *uppS-cdsA* operon

(A) Genome map showing the location and frequency of transposon insertion events that restore the viability of a *yhcB* mutant under toxic growth conditions: LB supplemented with vancomycin, or SDS and EDTA. (B) TIS data of the *uppS (ispU)* and *cdsA* operon. (Note that *uppS* is annotated as *ispU* in the BW25113 reference genome). Red and blue data correspond with the transposon orientation at the point of insertion. The height of the bar corresponds with mapped sequencing read frequency, capped at 20 in these images. The red boxes underneath each suppressor dataset represent significant differential abundance of insertions of the condition compared to the control, identified by AlbaTraDIS.

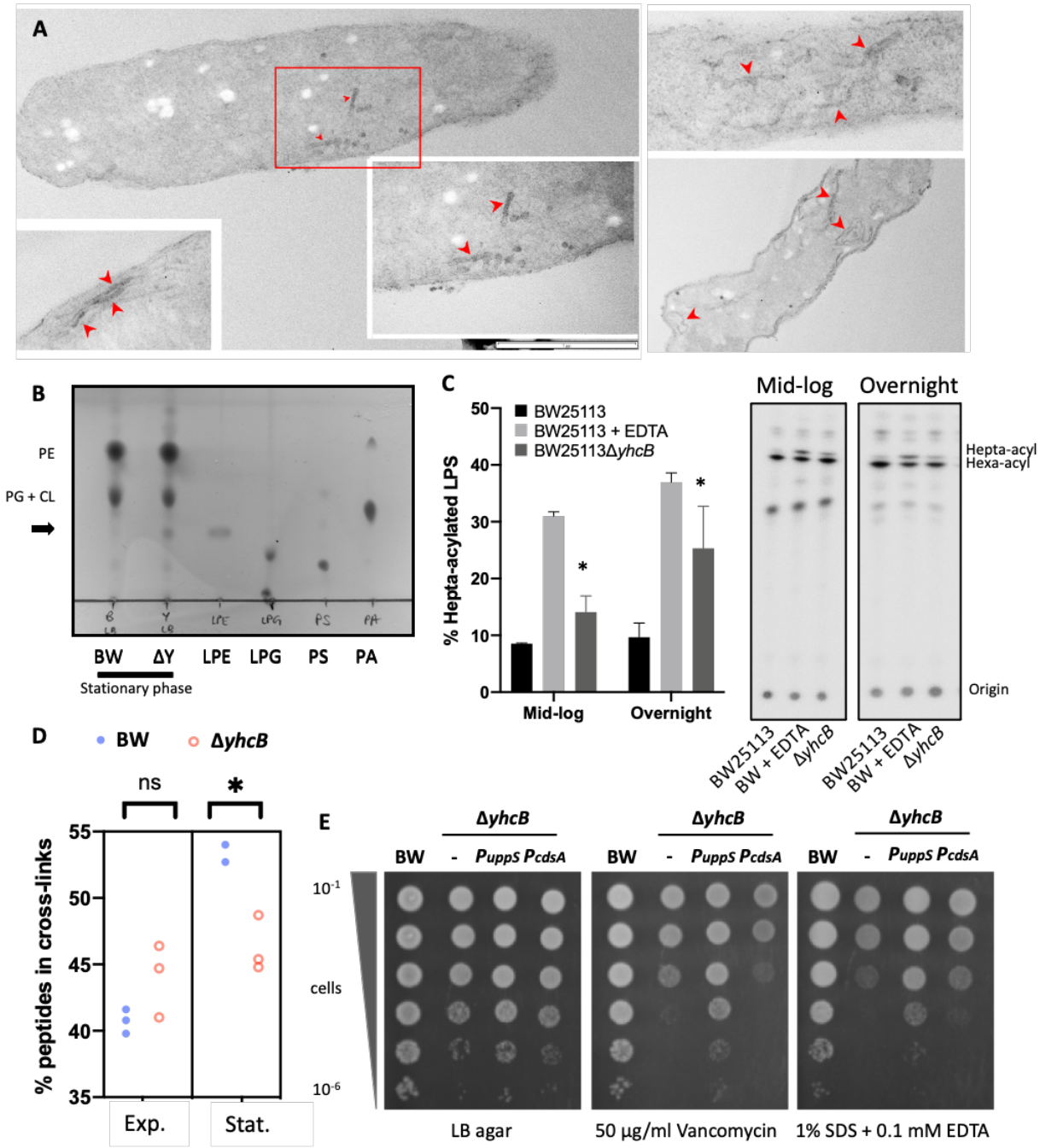

Figure 10. The *yhcB* mutant contains extra membrane and has an altered cell envelope

(A) Transmission electron micrograph of a Δ*yhcB* mutant cell with membrane ruffles indicated by red arrows. Scale bar = 1 µm. Additional whole cell images are in Fig. S10. (B) Phospholipid species extracted from BW25113 (BW) and the Δ*yhcB* mutant (ΔY) grown in LB broth until stationary phase and separated by thin layer chromatography (TLC) using a chloroform:methanol:water (65:25:4) solvent system. Standards of lysophosphatidylethanolamine (LPE), lysophosphatidylglycerol (LPG), phosphatidylserine (PS) and phosphatidic acid (PA) were loaded alongside for comparison. The additional spot in the ΔY sample is indicated with an arrow. (C) TLC/autoradiographic analysis of [^{32}P]-labeled lipid A extracted from mid-logarithmic growth and overnight growth cultures of BW25113 and Δ*yhcB* strains grown in LB. As a positive control for lipid A palmitoylation, BW25113 cells were treated with 25 mM EDTA for 10 min prior to extraction. The mean percentage of hepta-acylated lipid A and standard deviation were calculated from samples prepared in triplicate. Student's *t*-tests: *$P < 0.05$

compared with BW25113. (D) Comparison of the percentage of peptides in peptidoglycan crosslinks between strains at two stages of growth. Unpaired t-test with Welch's correction: *$P < 0.05$. Exponential phase cells were collected at an OD of 0.4, Stationary phase cells were harvested after 16 h at an OD of ~4.0. (E) Day cultures of BW25113; Δ*yhcB;* Δ*yhcB PuppS* and Δ*yhcB PcdsA* strains grown in LB for 5 h, normalised to an OD_{600} of 1.00 and 10-fold serially diluted before inoculating LB agar plates supplemented with vancomycin or SDS and EDTA. Abbreviations: Phosphatidylethanolamine (PE); Phosphatidylglycerol (PG); Cardiolipin (CL); Exponential phase (Exp.); Stationary phase (Stat.).

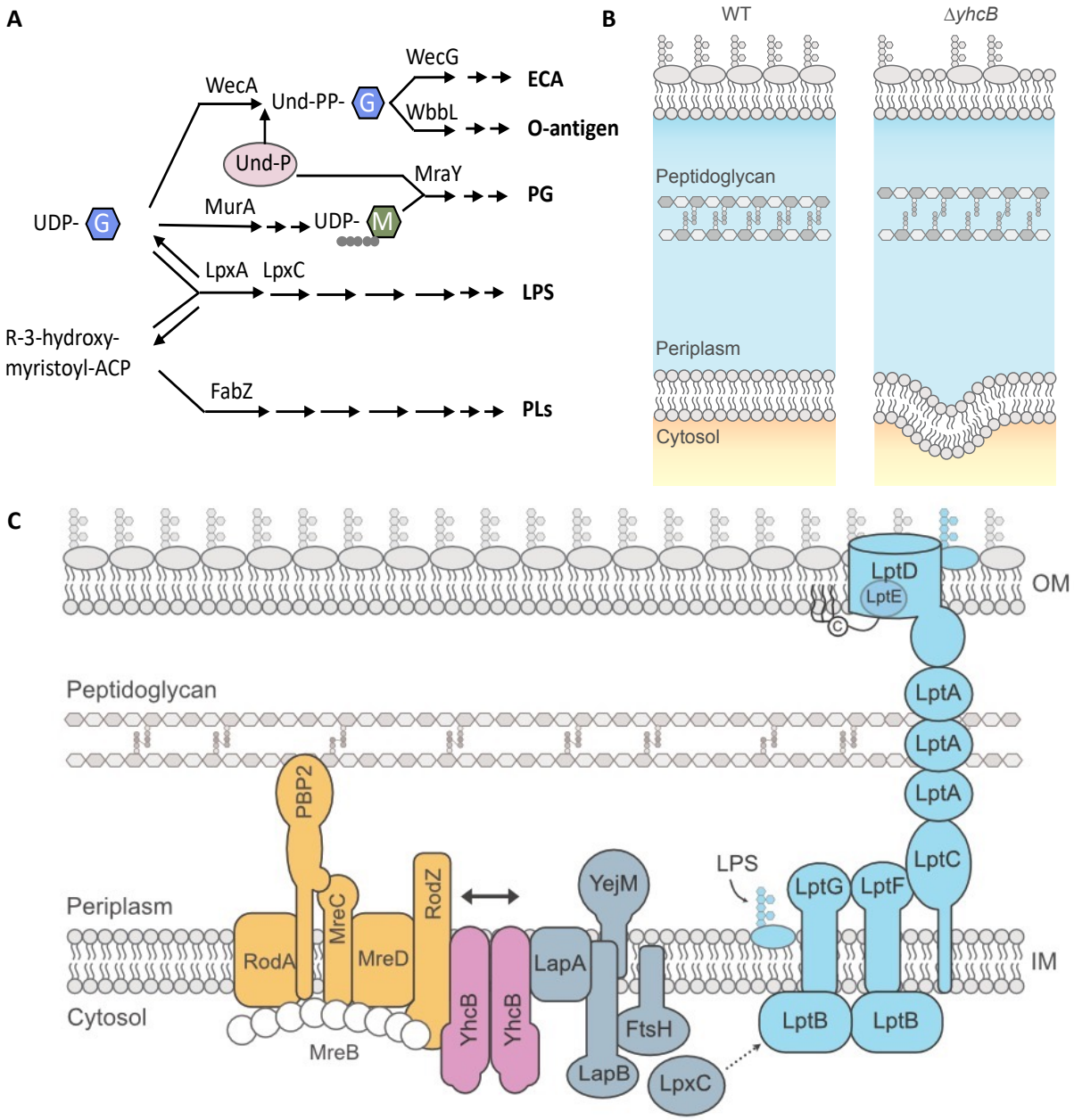

Figure 11. The pathways of cell envelope biosynthesis and relationship with YhcB (A) Schematic overview of the relationships between the biosynthetic pathways of individual components of the cell envelope. (B) A schematic of the imbalanced cell envelope of a *yhcB* mutant in comparison to wildtype (WT). The *yhcB* mutant suffers from defects in OM asymmetry, excessive phospholipid synthesis and altered crosslinking in the peptidoglycan layer. (C) The positional context of YhcB in conjunction with the reported protein interaction partners of YhcB *in situ*. YhcB interacts with both the elongasome (depicted here as mediated via RodZ, but YhcB is reported to interact with RodA, MreD and MreC in addition to RodZ) and LapA from the complex that regulates LpxC degradation. YhcB is spatially positioned to coordinate peptidoglycan expansion with LPS export. Abbreviations: Enterobacterial Common Antigen (ECA); Lipopolysaccharide (LPS); Peptidoglycan (PG); Phospholipid (PL); Undecaprenyl phosphate (Und-P); Undecaprenyl diphosphate (Und-PP); Uridine diphosphate (UDP); N-acetylglucosamine (G); N-acetylmuramic acid (M); Acyl Carrier Protein (ACP).

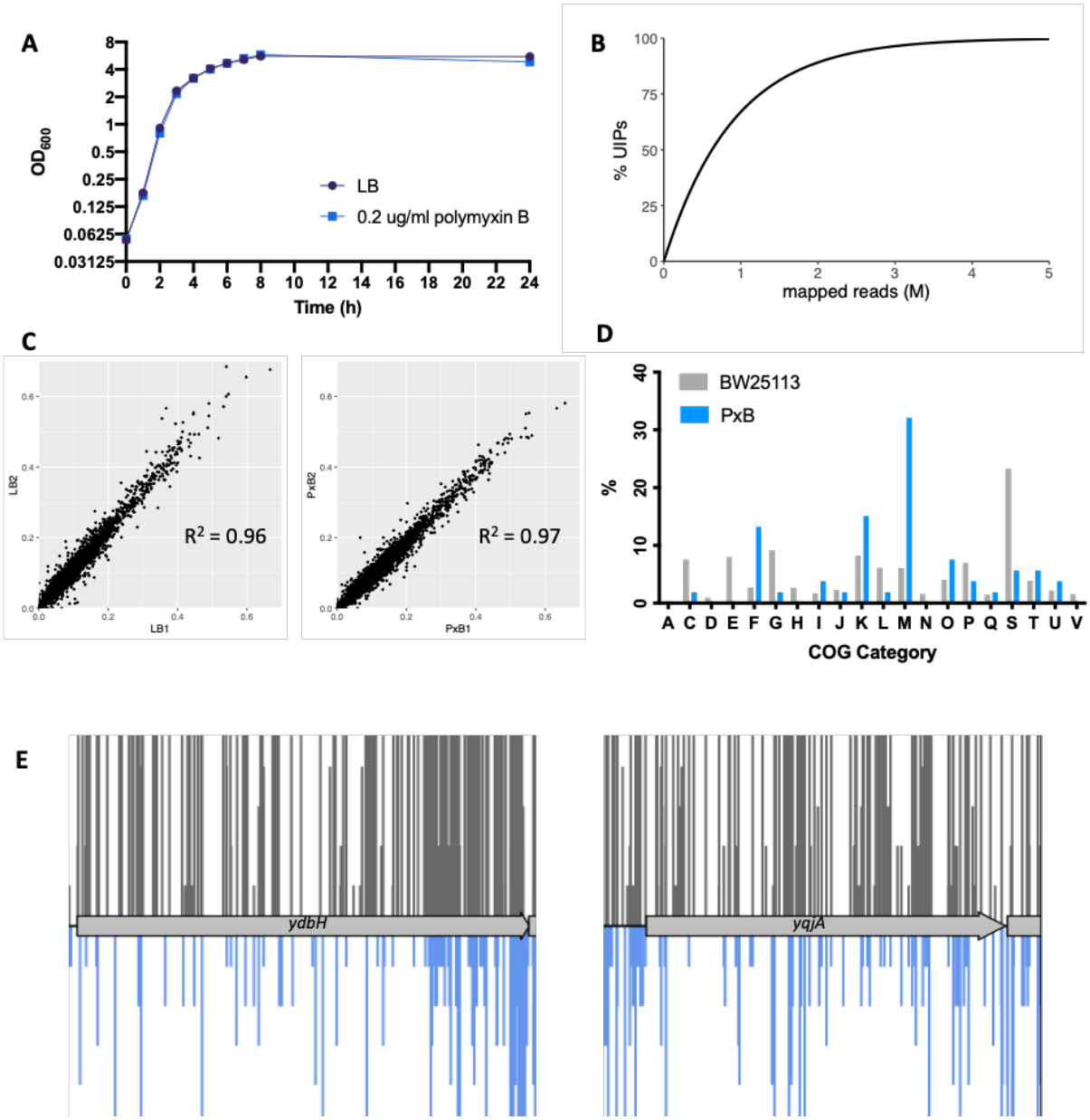

Supplementary Figure 1. Screening the BW25113 transposon library in sub-inhibitory concentrations of polymyxin B

(A) 0.2 µg/ml of polymyxin B in 50 ml LB does not inhibit growth of *E. coli* BW25113, under the conditions used to screen the library. One representative growth curve is shown, consistent with 5 repeats. (B) Calculation of the number of mapped reads needed to sample a given percentage of the transposon library. The equation $\mathrm{I} = s - s(\frac{s-1}{s})^n$ was used to estimate the number of mapped reads required to sample a given proportion of the dataset. s = 1,000,000 was taken as the total number of possible mutants (total transposon insertion sites). I = insertions identified, n = number of mapped reads. This data was used to calculate the approximate percentage of unique insertions identified for a given number of mapped reads, for a library of 1,000,000 unique mutants. (C) Comparison of insertion index scores (a measure of insertion density) per gene for each replicate of the library either exposed to LB only, or LB supplemented with polymyxin B. The scatter plots show the correlation coefficient for insertion density of each gene between replicates. (D) The relative abundance of Cluster of Orthologous Groups (COG) categories for all genes of BW25113 (grey) and for the 54 genes identified as required for growth in sub-inhibitory concentrations of polymyxin B (PxB; blue). (E) The transposon insertion profiles of *yqjA* and *ydbH* following outgrowth in LB only (grey, above) or in LB

1465 supplemented with polymyxin B (blue, below). The transposon insertion position along
1466 each gene is marked by a vertical line. The vertical line size corresponds with read depth,
1467 with visibly fewer transposon-insertion sites identified within *ydbH* and *yqjA* following
1468 outgrowth in polymyxin B.
1469

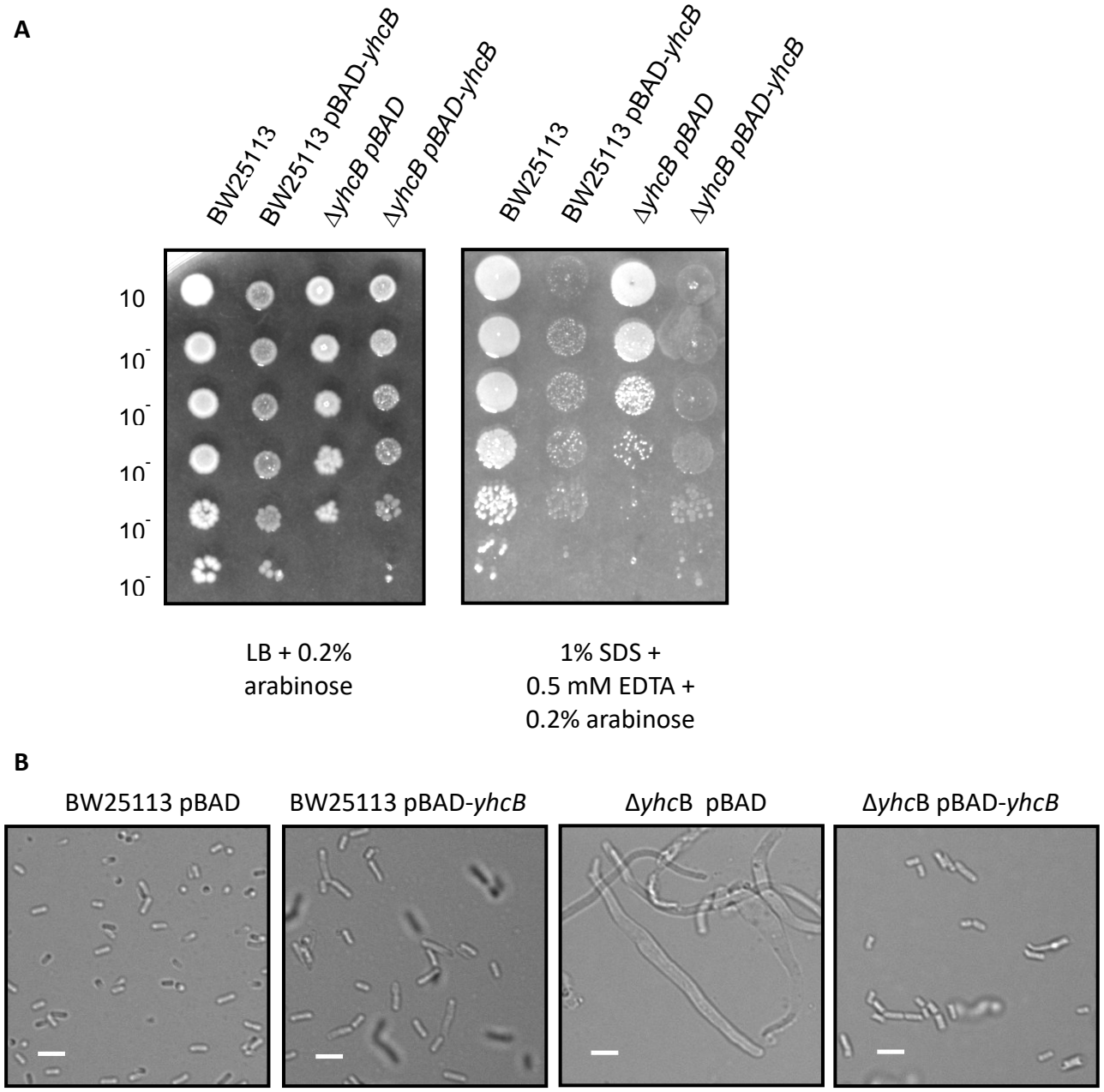

Supplementary Figure 2. Complementation of a Δ*yhcB* defect
(A) 10-fold serial-dilution of overnight cultures grown in LB, inoculated onto LB agar plates supplemented with 0.2% arabinose, with and without 1% SDS + 0.5 mM EDTA. Strains are carrying a pBad-Myc-His-A with or without the *yhcB* CDS under the control of an arabinose promoter. (B) DIC microscopy images of day cultures grown in LB supplemented with 0.4% arabinose and 100 µg/ml carbenicillin (to maintain plasmids), with a 5 µm scale bar for reference.

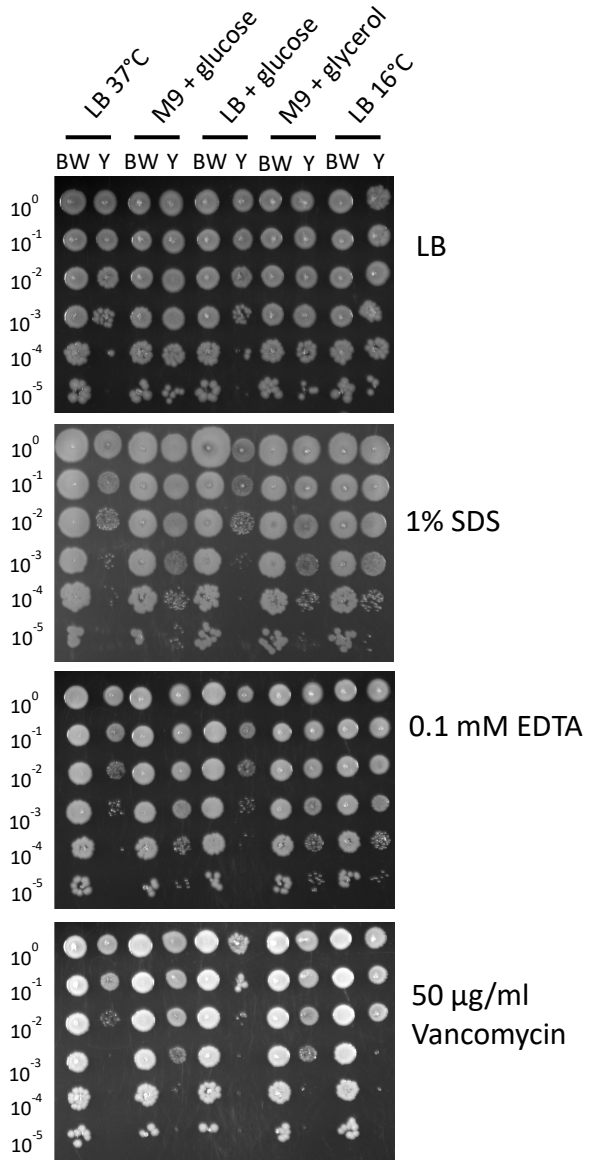

Supplementary Figure 3. The effect of different growth media on phenotype
10-fold serial-dilution of overnight cultures of the parent strain *E. coli* BW25113 (BW) and Δ*yhcB* strain (Y) grown to late stationary phase under different conditions (LB at 37˚C; M9 + 0.4% glucose at 37˚C; LB + 0.4% glucose at 37˚C; M9 + 0.4% glycerol at 37˚C; LB at 16˚C) normalized to an OD_{600} of 1.00 and inoculated onto LB agar plates supplemented with and without 1% SDS; 0.1 mM EDTA or 50 µg/ml vancomycin.

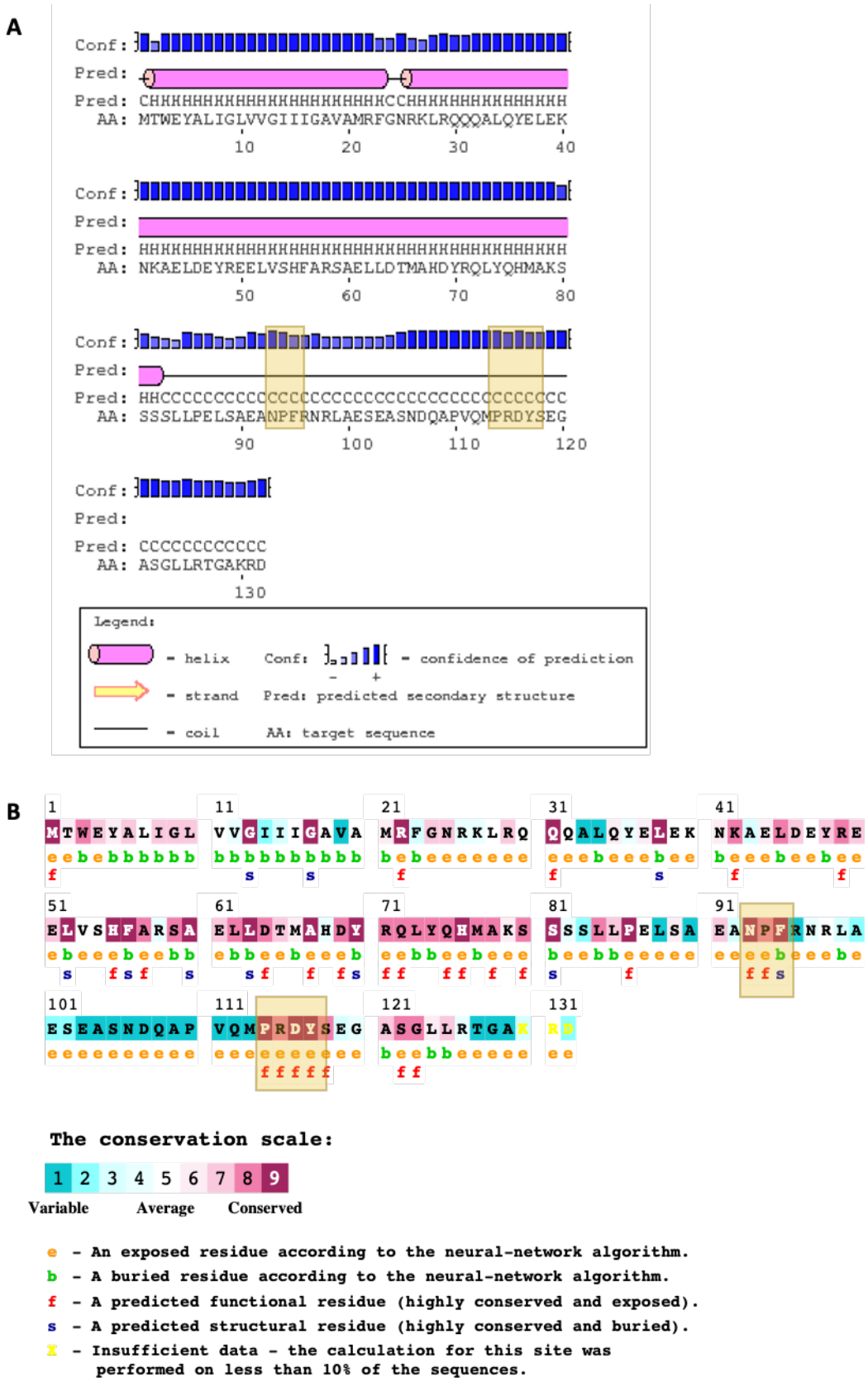

Supplementary Figure 4. Domains and conserved motifs of YhcB
(A) PSIPRED secondary structure prediction of YhcB (B) Conserved residues of YhcB predicted by ConSurf. Conserved 'NPF' and 'PRDY' motifs are highlighted with amber boxes in both panels.

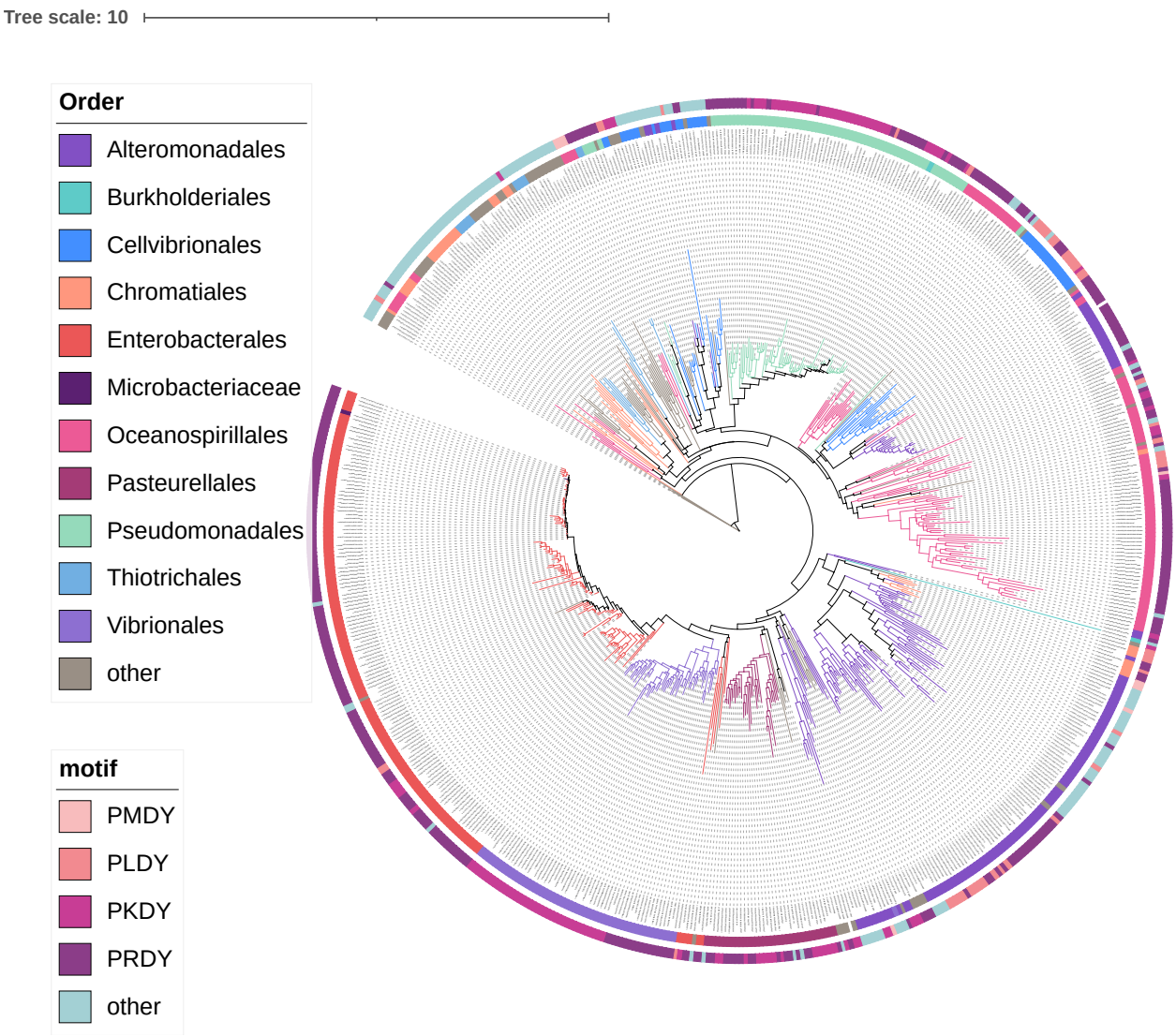

Supplementary Figure 5. Conservation of the PRDY domain
Phylogenetic analysis displaying conservation of YhcB in bacterial reference genomes. Branches of the tree, and second outermost track, are coloured according to taxonomic Order. The outermost track is coloured according to the amino acid residues within the 'PXDY' domain conserved among species. The label 'other' represents those that had a different sequence to the four listed.

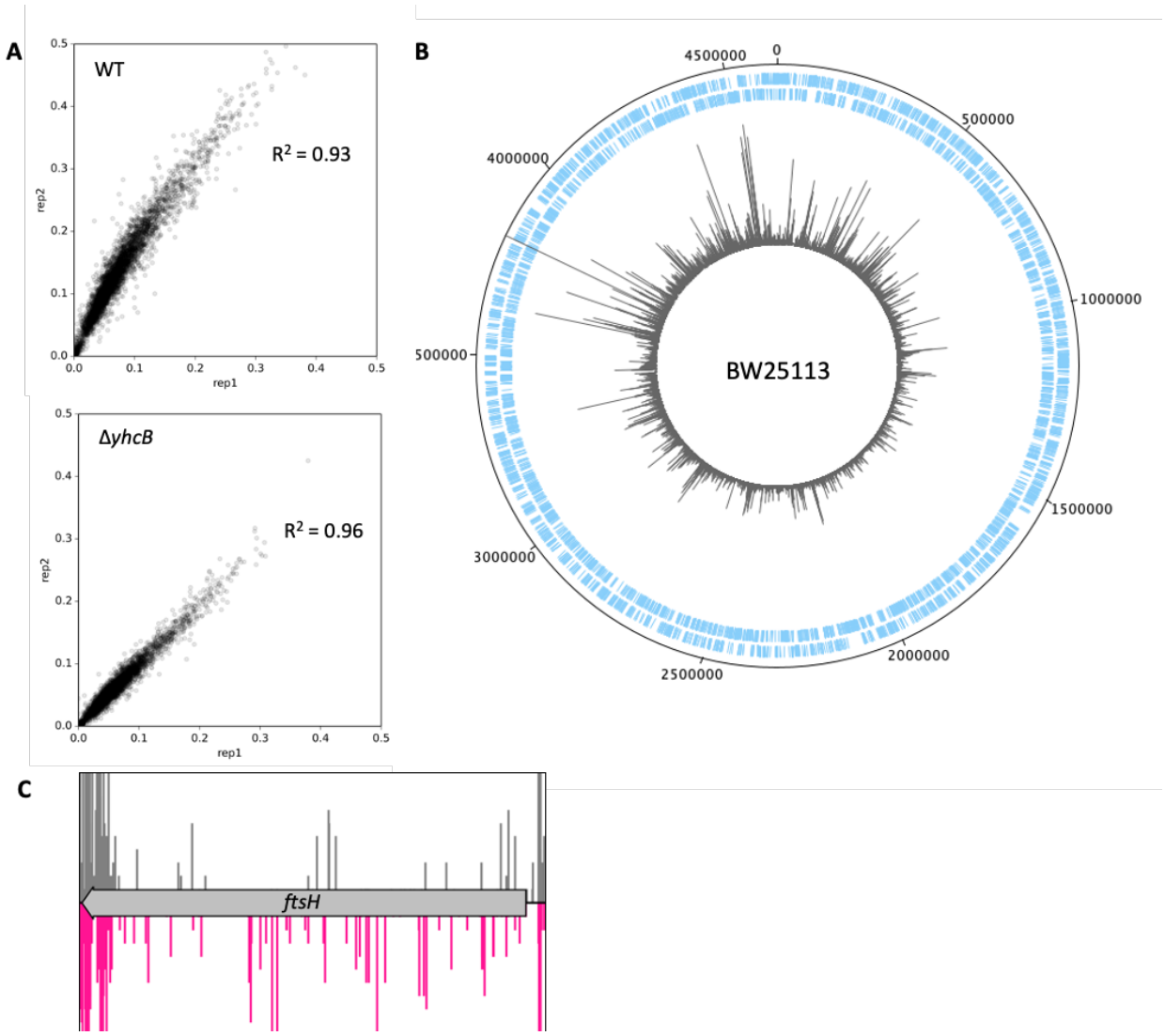

Supplementary Figure 6. Construction of a transposon library in BW25113 parent strain

(A) Comparison of insertion index scores (IIS) between technical replicates of each library. (B) The BW25113 transposon library. A genome map of BW25113 starting at the annotation origin, with the sense and antisense coding sequences of BW25113 shown in blue, respectively, and the position and frequency of sequenced transposon insertion events shown in grey. (C) The transposon insertion profile of *ftsH* shown for both libraries. Peaks represent the abundance of detected transposon insertion events for each library: WT (grey, above) and *yhcB* (pink, below) with read frequency capped at 10.

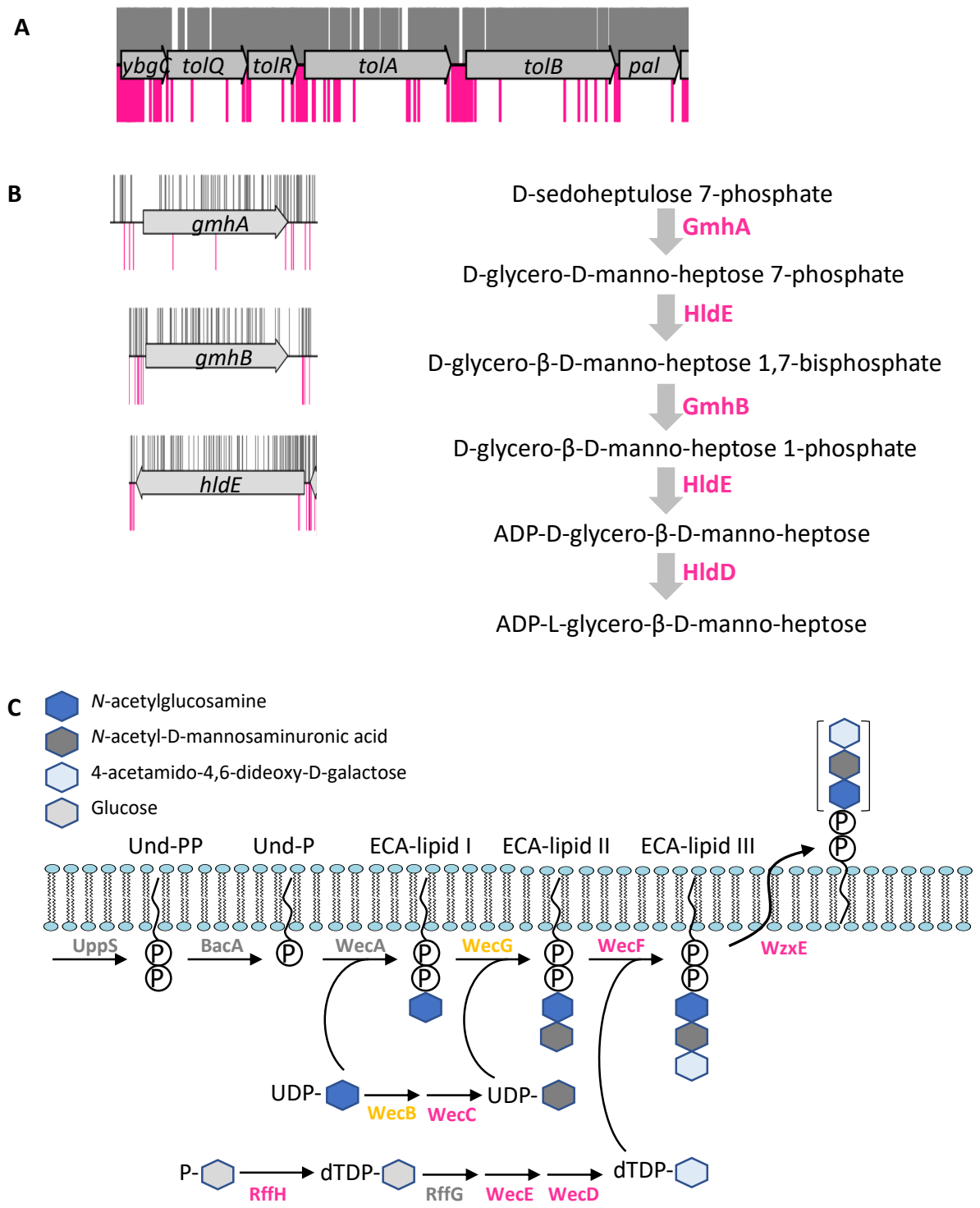

Supplementary Figure 7. Biosynthetic pathways required in a Δ*yhcB* background Transposon insertion data of the yhcB library shown in pink, below, control library shown in grey, above, the gene track with all insertion data capped at a frequency of 1. (A) Transposon insertion profile of the *tol-pal* operon. (B) The heptose biosynthetic pathway, required for LPS core biosynthesis. (C) Schematic of the ECA biosynthesis pathway adapted from Jorgenson *et al*. (2016). Abbreviations: Enterobacterial Common Antigen (ECA); Undecaprenyl phosphate (Und-P); Phosphate (P); Adenosine diphosphate (ADP); deoxythymidine diphosphate (dTDP); Uridine diphosphate (UDP).

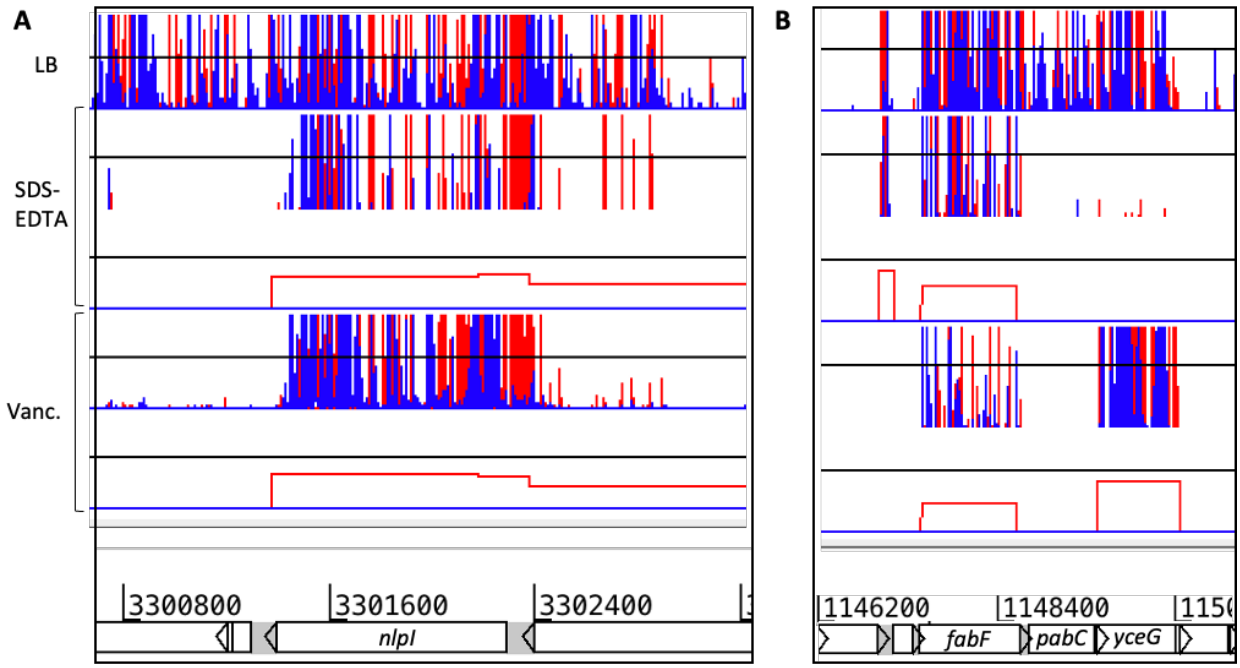

Supplementary Figure 8. Transposon insertion sites within *nlpI* and *fabF* that restore resistance of a *yhcB* mutant to vancomycin or SDS and EDTA.
Transposon insertion data for suppressor screens. Red and blue vertical lines indicate the transposon insertion position and correspond with the transposon orientation at the point of insertion. The height of the bar corresponds with mapped sequencing read frequency. The top track represents data for the library plated on LB. The tracks underneath represent the Δ*yhcB* transposon library plated on LB supplemented with SDS and EDTA, or vancomycin, at lethal doses to the BW25113Δ*yhcB* parent strain. The red boxes underneath each suppressor dataset represent significant differential abundance of insertions in the condition sample compared to the control, identified by AlbaTraDIS.

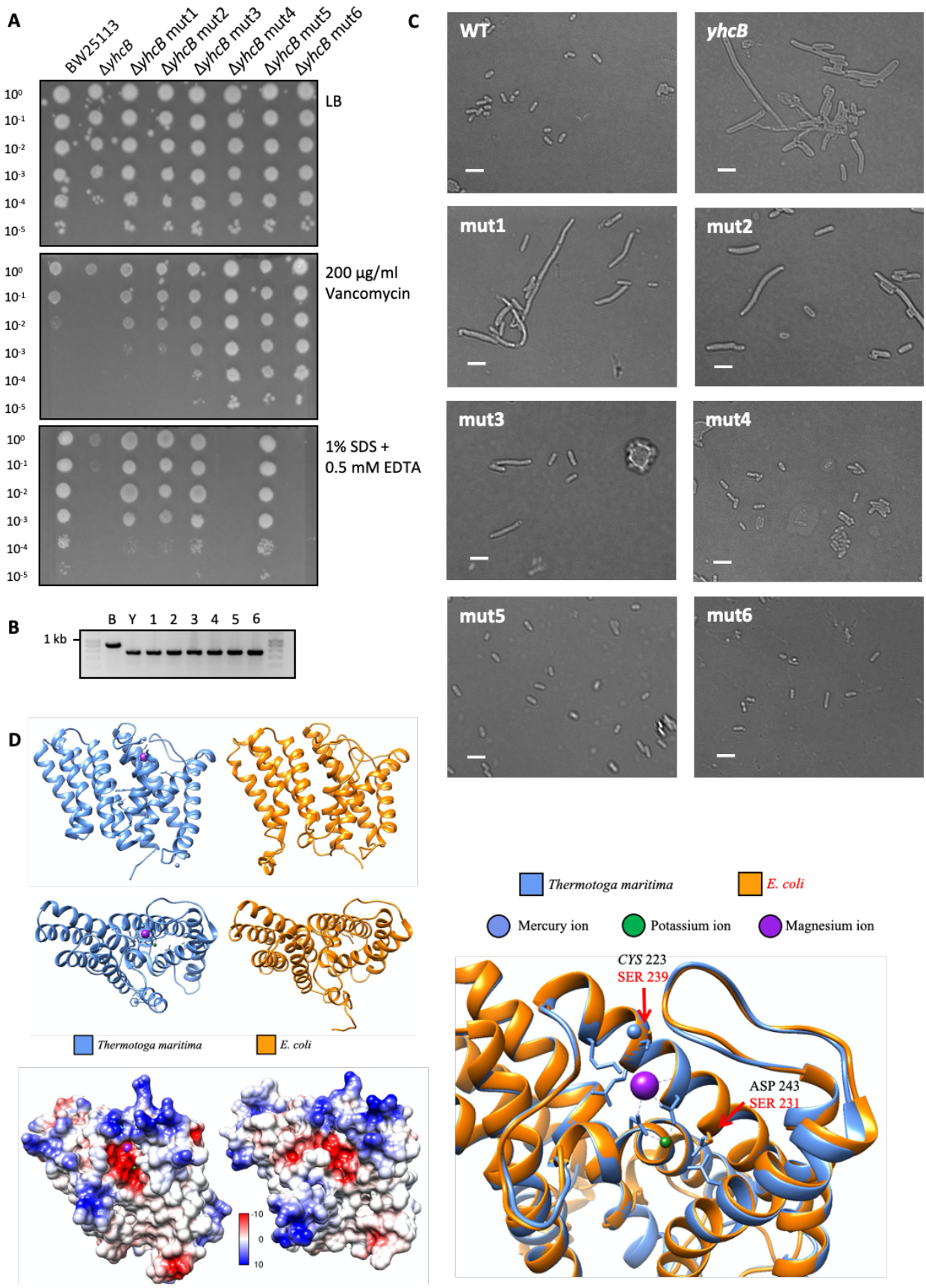

Supplementary Figure 9. Natural suppressor mutations that are restorative in a

***yhcB* mutant**

(A) Validation of natural suppressor mutants. 10-fold serial dilutions of E. coli K-12 BW25113, BW25113Δ*yhcB* and six BW25113Δ*yhcB* revertant suppressor mutants, grown on LB, LB supplemented with 200 µg/ml vancomycin, or 1% SDS + 0.5 mM EDTA. (B) PCR amplification of the *yhcB* locus to confirm *yhcB*-deletion in these strains. (C) DIC images of BW25113, BW25113Δ*yhcB* and six BW25113Δ*yhcB* revertant suppressor mutants grown overnight in LB. Scale bar of 5 µm. (D) Solved structure of *Thermatoga maritima* CdsA (blue) and the predicted structure of *E. coli* CdsA (orange), with the surface electrostatic potential of each shown below. The deep red and deep blue colours indicate electronegative and electropositive regions at −10 and 10 $kT\,e^{-1}$, respectively. An overlay of the cation-binding pocket of CdsA from *T. maritima* and *E. coli* is shown in the bottom right panel. The equivalent mutated residues are annotated: shown in black, above for *T. maritima* and red, below for *E. coli*. Note the S223C residue mutated in *T. maritima* to achieve a resolved structure.

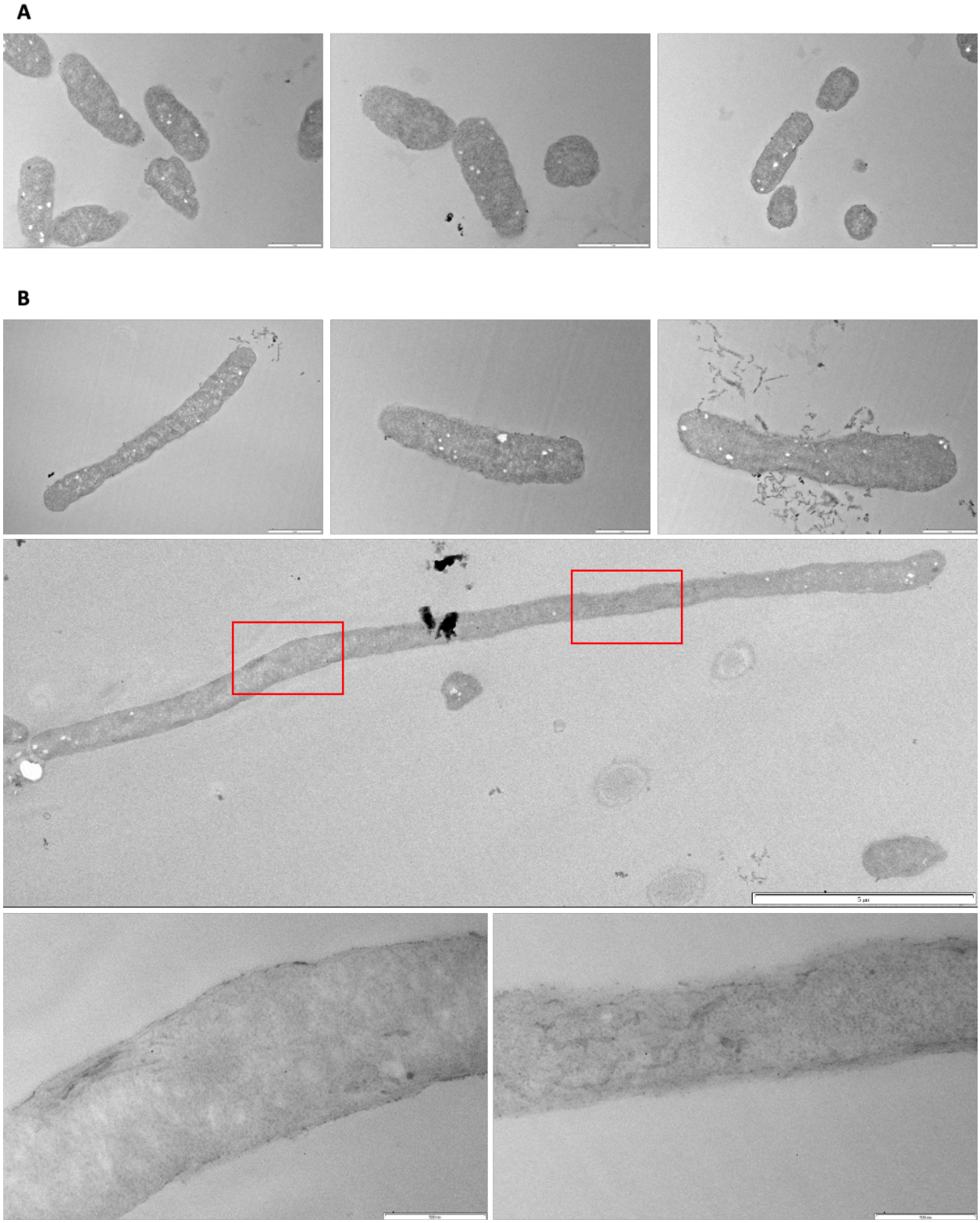

Supplementary Figure 10. TEM images of BW25113 and the Δ*yhcB* mutant
Transmission electron micrographs of (A) BW25113 and (B) the Δ*yhcB* mutant cells. Scale bar = 1 μm in the top six images. A large Δ*yhcB* mutant cell is shown with a scale bar of 5 μm and two regions of excess or ruffled membrane structures are highlighted by red boxes (annotated in Fig. 10A); enlarged images of these sections are shown underneath with a scale bar of 500 nm each.

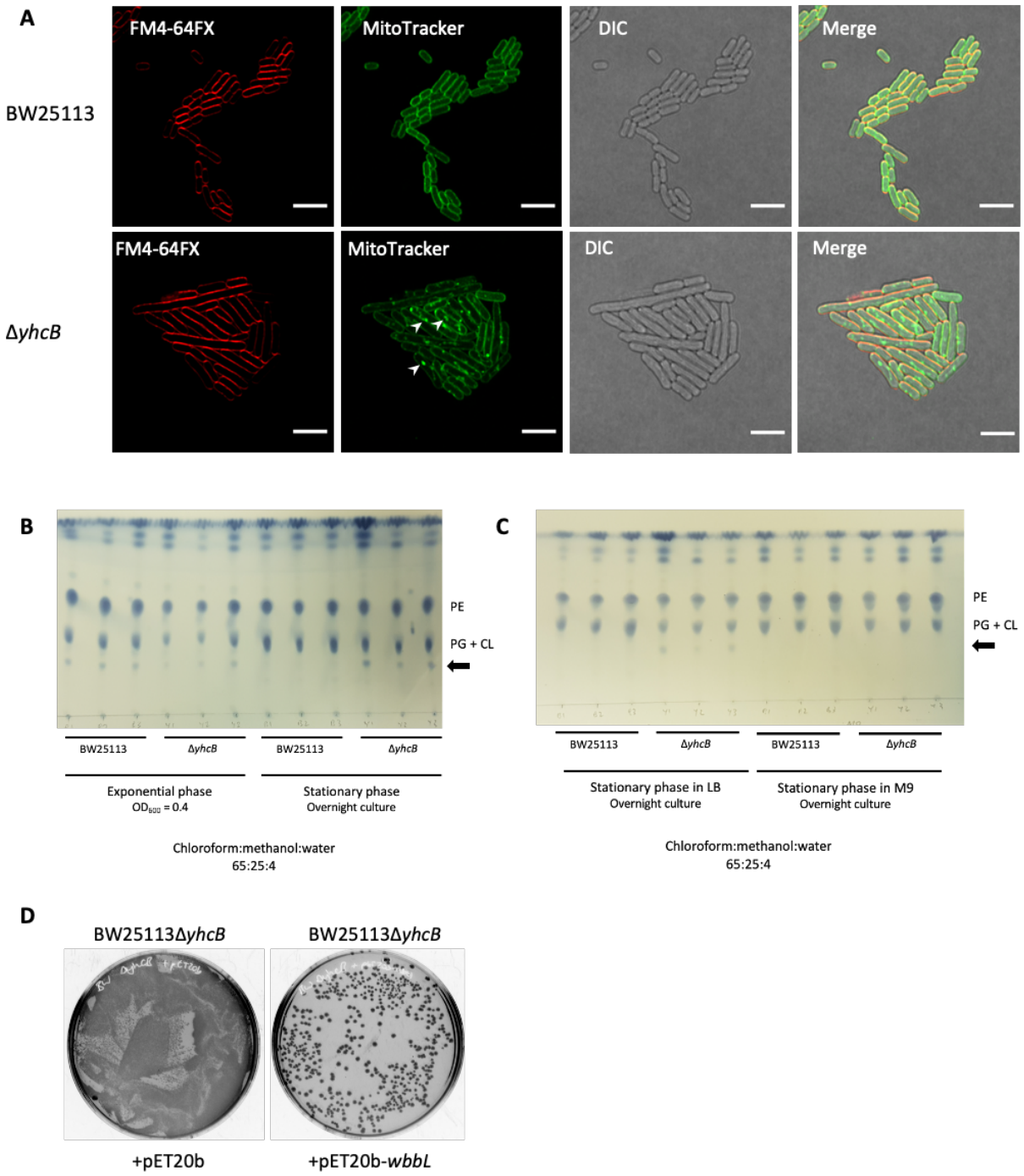

Supplementary Figure 11. The *yhcB* mutant contains extra membrane, has an altered cell envelope and restoration of O-antigen is toxic

(A) *E. coli* K-12 BW25113 and BW25112Δ*yhcB* grown in LB, labelled with FM4-64FX and MitoTracker Green FM. Images were taken at 3 h and are representative of n = 3 experiments. Lipid accumulation is indicated by the white arrows. Scale bar of 5 µm. (B-C) Thin layer chromatography (TLC) separation of phospholipid species in chloroform:methanol:water (65:25:4) solvent system, and stained with PMA. (B) Samples grown in LB and collected at two stages of growth. (C) Samples grown overnight in LB or M9-glucose. (D) Transformation efficiency of pET20b constructs +/- *wbbL* for restoring O-antigen in a Δ*yhcB* mutant. Abbreviations: Phosphatidylethanolamine (PE); Phosphatidylglycerol (PG); Cardiolipin (CL).

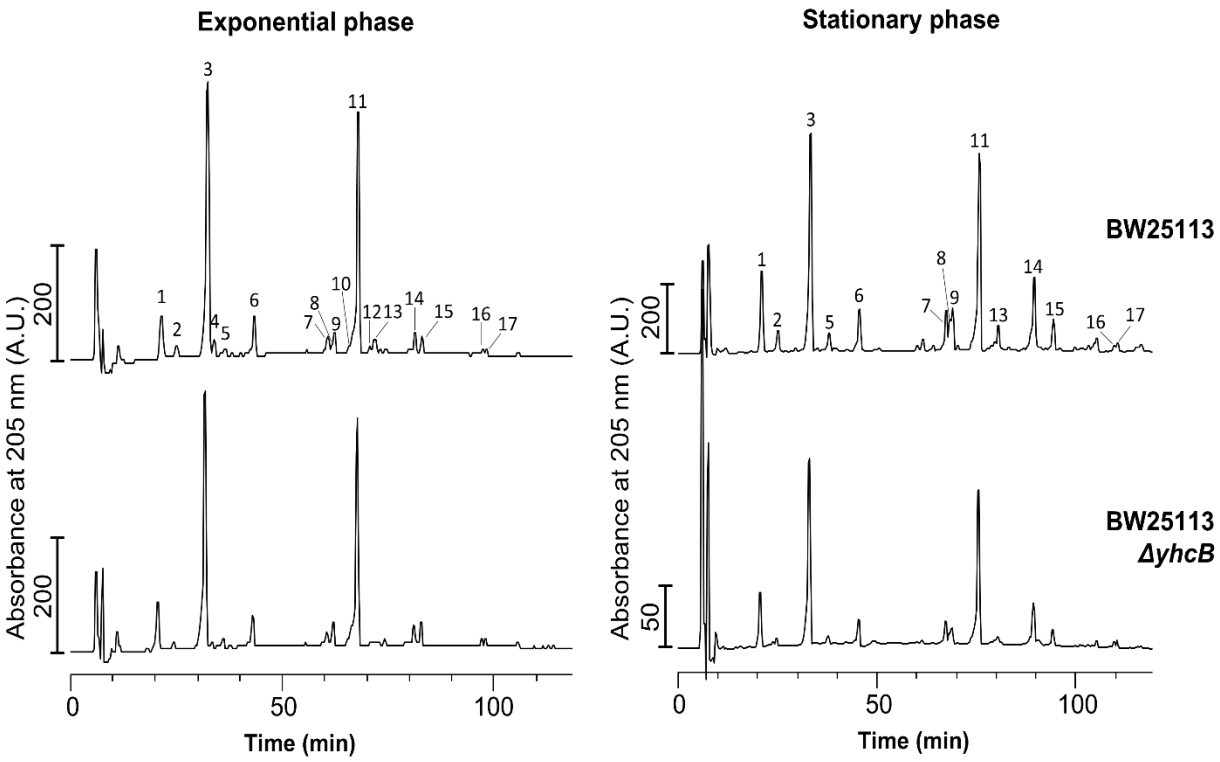

Supplementary Figure 12. Analysis of the peptidoglycan composition
Representative HPLC chromatograms showing the muropeptide composition of BW25113 and BW25113Δ*yhcB* at exponential and stationary phase. Purified peptdoglycan was digested with cellosyl and the resulting muropeptides were reduced with sodium borohydride and separated by HPLC. The major muropeptides (No. 1-17) are quantified in Table S5.

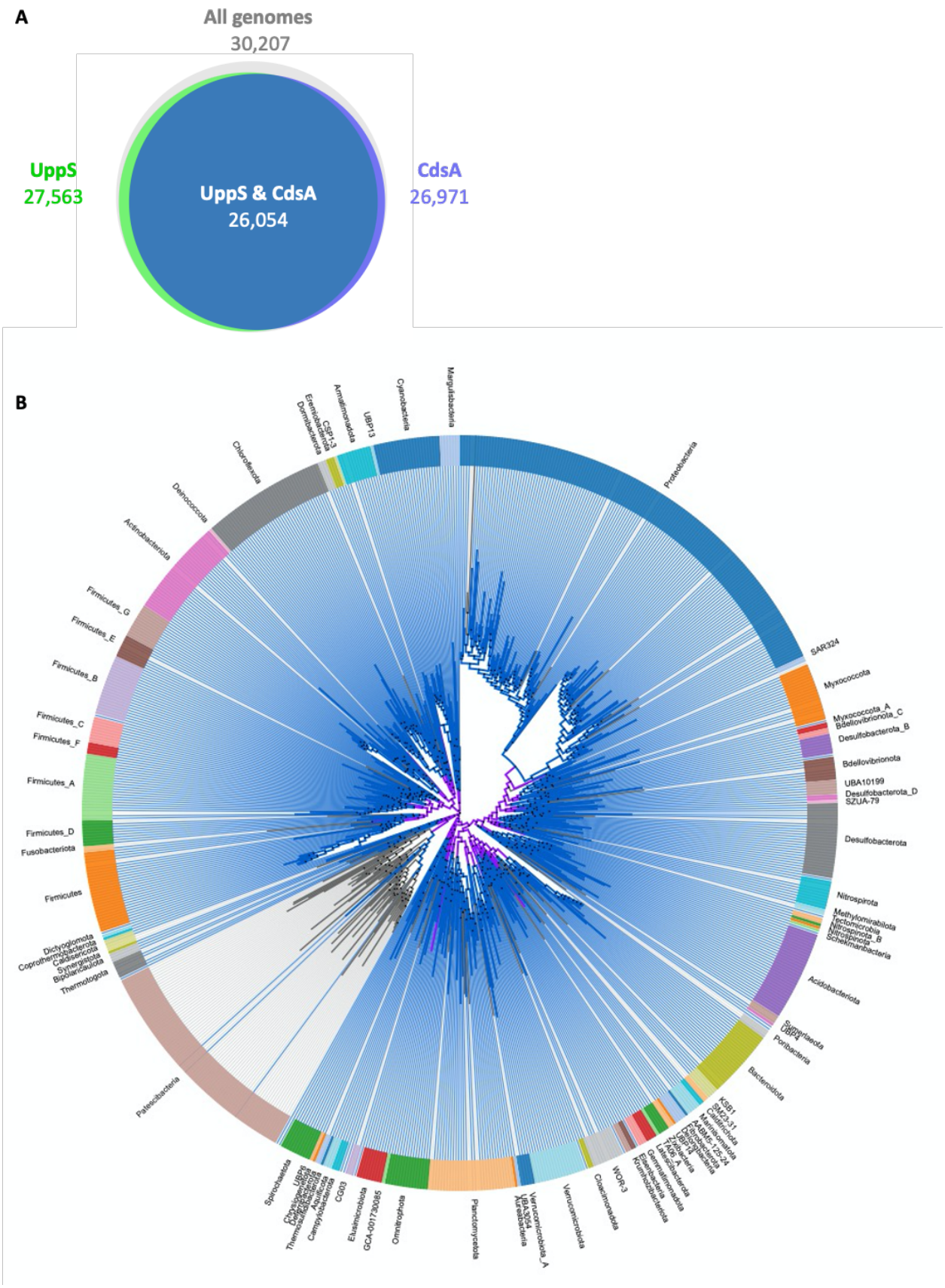

Supplementary Figure 13. UppS and CdsA conservation

(A) The number, and overlap, of bacterial genomes containing a UppS (K00806) or CdsA (K00981) homolog obtained from AnnoTree (v1.2.0) using the KEGG identifiers and the following search criteria: % identity: 30; E value: 0.00001; % subject alignment: 70; % query alignment: 70. (B) Tree representation of the phylogeny of bacterial genomes with species containing both UppS and CdsA highlighted in blue.

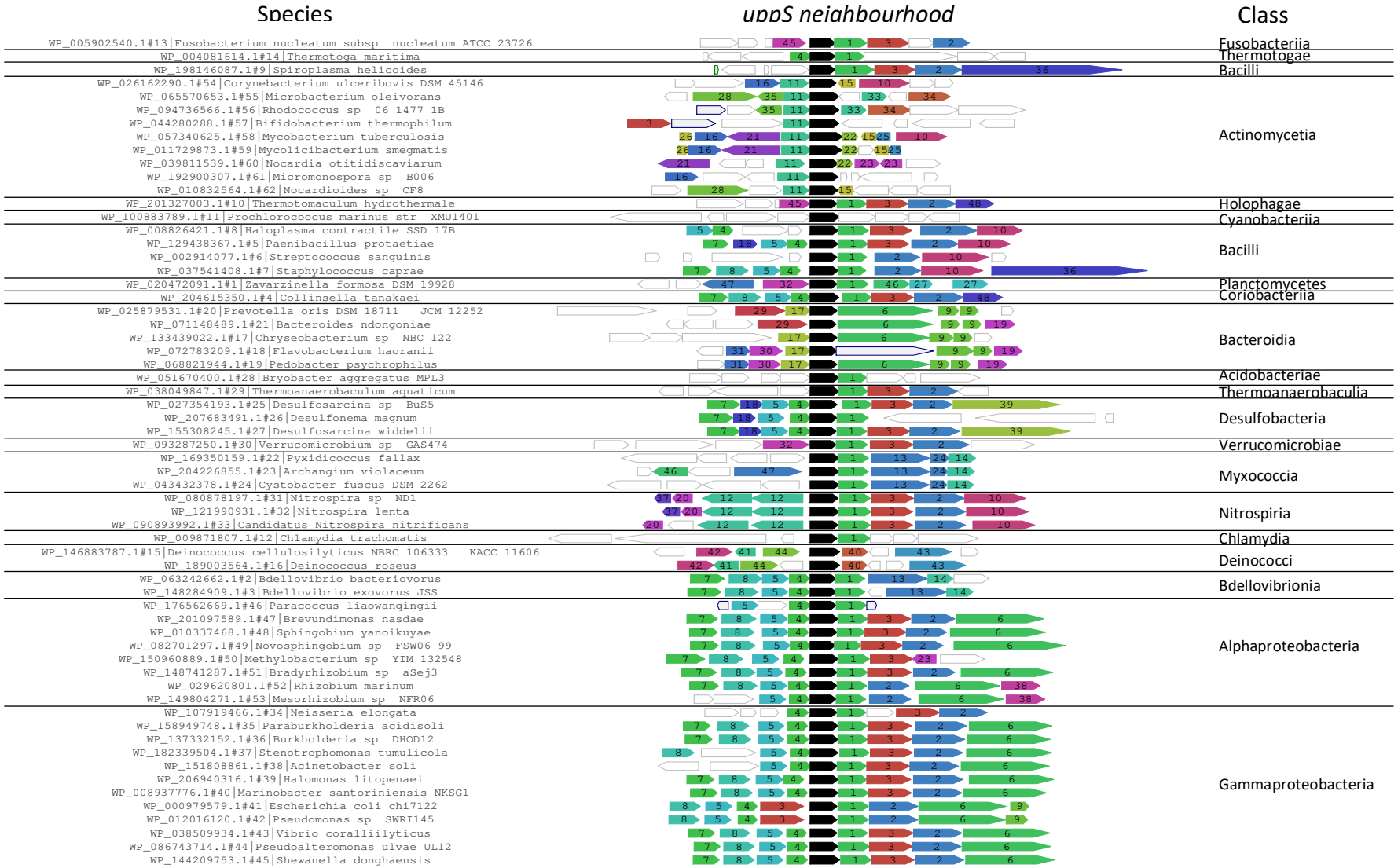

Supplementary Figure 14. *uppS* and *cdsA* neighbourhood conservation across the bacterial kingdom

The conservation of the *uppS* gene neighbourhood represented by 62 diverse bacterial species. *uppS* is depicted in black, and *cdsA* in green (1). The remaining gene identifiers can be found in Supplementary Table 9. Data calculated using FlaGs (Saha et al. 2020).

1600 **Supplementary Tables**
1601
1602 Supplementary Table 1. Polymyxin B TIS screen data
1603 Supplementary Table 2. Transposon library construction metrics
1604 Supplementary Table 3. Insertion index scores of the *yhcB* and WT transposon libraries
1605 Supplementary Table 4. Gene fitness in a *yhcB* mutant strain
1606 Supplementary Table 5. Peptidoglycan composition
1607 Supplementary Table 6. PANTHER analysis
1608 Supplementary Table 7. AlbaTraDIS identification of suppressor mutations
1609 Supplementary Table 8. Mutations identified in spontaneous revertant suppressor
1610 mutants
1611 Supplementary Table 9. FlaGs gene identifiers